

## Accepted Manuscript

Contributions of U-Th-Pb dating on the diagenesis and sediment sources of the Lower Group (BI) of the Mbuji-Mayi Supergroup (Democratic Republic of Congo)

C. François, B.K. Baludikay, J.Y. Storme, D. Baudet, J.L. Paquette, M. Fialin, E.J. Javaux

PII: S0301-9268(17)30117-1

DOI: <http://dx.doi.org/10.1016/j.precamres.2017.06.012>

Reference: PRECAM 4794

To appear in: *Precambrian Research*

Received Date: 13 March 2017

Revised Date: 8 June 2017

Accepted Date: 12 June 2017

Please cite this article as: C. François, B.K. Baludikay, J.Y. Storme, D. Baudet, J.L. Paquette, M. Fialin, E.J. Javaux, Contributions of U-Th-Pb dating on the diagenesis and sediment sources of the Lower Group (BI) of the Mbuji-Mayi Supergroup (Democratic Republic of Congo), *Precambrian Research* (2017), doi: <http://dx.doi.org/10.1016/j.precamres.2017.06.012>

This is a PDF file of an unedited manuscript that has been accepted for publication. As a service to our customers we are providing this early version of the manuscript. The manuscript will undergo copyediting, typesetting, and review of the resulting proof before it is published in its final form. Please note that during the production process errors may be discovered which could affect the content, and all legal disclaimers that apply to the journal pertain.



**Contributions of U-Th-Pb dating on the diagenesis and sediment sources of the  
Lower Group (BI) of the Mbuji-Mayi Supergroup (Democratic Republic of Congo)**

C.François<sup>1</sup>, B.K. Baludikay<sup>1</sup>, J.Y.Storme<sup>1</sup>, D.Baudet<sup>2</sup>, J.L.Paquette<sup>3</sup>, M.Fialin<sup>4</sup> & E.J.Javaux<sup>1</sup>

<sup>1</sup> *Paleobiogeology-Paleobotany-Paleopalynology Lab, Department of Geology, UR Geology, B18, University of Liege, 4000 Liège, Belgium*

<sup>2</sup> *Geodynamics and Mineral Resources Service, Royal Museum for Central Africa, Tervuren, Belgium*

<sup>3</sup> *Laboratoire Magmas & Volcans, Université Clermont Auvergne, CNRS-IRD-OPGC, 63000 Clermont-Ferrand, France*

<sup>4</sup> *Camparis, Université Paris 6, 4 place Jussieu, 75252 Paris Cedex 5, France*

\*Corresponding author. Tel.: +3243669411. E-mail address: [c.francois@ulg.ac.be](mailto:c.francois@ulg.ac.be) (C. François).

**Abstract**

In this paper, we present new age constraints for the lower part of the Meso-Neoproterozoic sedimentary Mbuji-Mayi Supergroup (Democratic Republic of Congo, DRC). This Supergroup preserves a large diversity of organic-walled microfossils, evidencing the diversification of early eukaryotes for the first time in Central Africa. We use different methods such as *in situ* U-Pb geochronology by LA-ICP-MS and U-Th-Pb chemical datings by Electron Microprobe on diagenetic and detrital minerals such as xenotimes, monazites and zircons. We attempt to better constrain the provenance of the Mbuji-Mayi sediments and the minimum age of the Mbuji-Mayi Supergroup to constrain the age of the microfossils. Results with LA-ICP-MS and EMP provide new ages between 1030 and 1065 Ma for the diagenesis of the lower part of the sedimentary sequence. These results are consistent with data on biostratigraphy supporting the occurrence of worldwide changes at the Mesoproterozoic/Neoproterozoic boundary.

## 1. Introduction

The Mbuji-Mayi Supergroup (former “Système de la Bushimay”), DRC, (**Figs.1 & 2**) located between the Archean-Paleoproterozoic Congo-Kasai Craton and the Mesoproterozoic Kibara Belt, consists of a sedimentary sequence unaffected by regional metamorphism during this long history (*Raucq, 1957; 1970; Baludikay et al., 2016b*). Recently, a large diversity of well-preserved acritarchs (organic-walled microfossils) was described including a total of 49 taxa belonging to 27 genera (*Baludikay et al., 2016a*). This microfossil assemblage comprises 11 species of unambiguous eukaryotes, 10 species of possible eukaryotes or prokaryotes and 28 species of probable bacteria, attesting for the first time the diversification of complex life (early eukaryotes) in Meso/Neoproterozoic redox stratified oceans of Central Africa. The Mbuji-Mayi Supergroup did not suffer high metamorphism and deformation due to its location within the broad Congo-Kasai Craton, away from the Pan-African orogeny that developed at its margin during the final amalgamation of Gondwana. These favorable conditions permitted a good preservation of the microfossils and also of the diagenetic minerals. Dating this Supergroup has been and is still a challenge despite several attempts. Recently, *Delpomdor et al. (2013)* provided a maximum age for the lower part of the Supergroup (BI Group) only based on detrital zircon ages. In this study, we combine different geochronological methods, in particular on diagenetic minerals such as monazite and xenotime but also on detrital zircons. Our new results permit to provide better constraints on the age of the Mbuji-Mayi Supergroup, on the complex timing and source of sediments filling the basin, of its microfossil assemblage, and importantly, on the diversification of early eukaryotes in central Africa.

## 2. Geological setting of Mbuji-Mayi Supergroup

The Mbuji-Mayi Supergroup is located in the Sankuru-Mbuji-Mayi-Lomami-Lovoy (SMLL) basin (**Fig.1**), an intracratonic failed-rift basin (*Kadima et al., 2011*) located at the northern part of the Congo-Kasai Craton (DRC) between 5°S and 9°S and 23°E and 26°E. This Archean/Paleoproterozoic craton was edged by the Kibara (1.4–1.0 Ga, in the northeast) and Irumide (ca. 1.02 Ga, in the southeast) orogenic belts (*Johnson et al., 2005; De Waele and Fitzsimons, 2007; De Waele et al., 2008; Begg et al., 2009; Fernandez-Alonso et al., 2012*). In this paper, we focused our work in the western part of the SMLL basin between the Dibaya Complex to the south (2.6-2.8 Ga; *Delhal et al., 1975; Cahen et al., 1984, Delpomdor et al., 2013*), corresponding to the northern part of the Congo-Kasai Craton, and the Mesoproterozoic Kibara Belt to the east.

Cores were drilled during the 1950's in the Sankuru-Mbuji-Mayi area, in several locations between the Lubi (East Kasai) and Luembe rivers (North Katanga; **Figs.1 & 2**) and are stored today in the collections of the Royal Museum for Central Africa (RMCA) in Tervuren (Belgium). Detailed

petrological descriptions of these drill cores were carried out by *Wazilewski (1953)* and *Raucq (1957, 1970)*, which allowed recognition of corresponding stratigraphic units. *Delpomdor (2013)* updated these descriptions using a newer sedimentological model.

The lithostratigraphy of the Supergroup consists of two Groups (**Fig.2**). The lower siliciclastic sequence (BI Group; ~ 500 m thick) is poorly age-constrained and approximatively dated between *ca.*  $1174 \pm 22$  Ma (*Delpomdor et al., 2013*) and *ca.* 1055 Ma (*Cahen et al., 1954; Holmes & Cahen, 1955; Raucq, 1957; Cahen, 1974*). It is unconformably overlying the *ca.* 2.8-2.6 Ga granitoid Dibaya Complex (*Delhal et al., 1975; Cahen et al., 1984, Delpomdor et al., 2013*). The upper carbonated sequence (BII Group; ~1,000 m-thick) is intercalated with sparse organic-rich shales and is partially covered by lavas dated around 950 Ma (*Cahen et al., 1974; Cahen et al., 1984*).

The sedimentary sequence is unaffected by regional metamorphism, temperatures recorded by the basin are lower than 300°C (*Raucq, 1957; 1970; Baludikay et al., 2016b*). Siliciclastic sequences (BI Group) are found in particular, in the S70 Tshinyama drill core (named hereafter “Lubi”; samples RG57624 to 57826 of the RMCA serial number collection) and Kafuku 15 drill core (named hereafter “Kafuku”; samples RG41330 to 41384). The BI Group consists of six Subgroups: BIa, BIb, BIc, BId, BIE and BIe. This Group is mostly siliciclastic, and starts with deposition in shallow water, with signs of emersion observed in the Lubi drill core (mudcracks and gypsum). Carbonated sequences (BII Group) are found in the Bena-Kalenda drill core, Kanshi S13B drill core (named hereafter “Kanshi”; samples RG32201 to RG32464), as well as Bena-Tshovu drill core (samples RG31534 to RG31646). The BII Group, including mainly transgressive carbonates, consists of five Subgroups: BIIa, BIIb, BIIc, BII d and BIIe. Detailed descriptions of these Subgroups have been given in *Raucq (1957, 1970)* and were updated (especially for the carbonates) by *Delpomdor (2013)* and *Delpomdor et al. (2015)*. The BII Group is alternately marked by the development of stromatolites interbedded with thin detrital levels or by thick layers of carbonates with cherts, corresponding to a long subsidence regime without terrigenous contributions (*Bertrand-Sarfati, 1972*). The regular intraformational breccias or conglomerates throughout the BII (b, c, and e) Group reflect the instability of the basin and its tendency of emersion in oxidizing environment (*Delhal & Ladmirant, 1979*).

Basaltic lavas topping the Mbuji-Mayi Supergroup in the northeast of the Mbuji-Mayi area (**Figs.1 & 2**) were dated at  $948 \pm 20$  Ma (*Cahen et al., 1974; Cahen et al., 1984*). The emplacement of these summital basalts marked the end of the sedimentary sequence.

### 3. Previous geochronological studies

The Mbuji-Mayi Supergroup unconformably overlies the *ca.* 2.9–2.6 Ga granitoid Dibaya Complex (**Figs.1 & 2**). This age was obtained by Rb-Sr method (whole rock) on migmatites and granites ( $2648 \pm$

22 Ma and  $2593 \pm 92$  Ma; *Delhal et al., 1975; Cahen et al., 1984*) and by U-Pb dating (ca. 2680 Ma on zircons, monazites and titanites; *Delhal et al., 1975; Cahen et al., 1984* and around 2.8–2.7 Ga on zircons; *Delpomdor et al., 2013*).

A thermo-tectonic event was dated at ca. 2000–2200 Ma (*Cahen et al. 1984*) by Rb-Sr method on muscovite from micaschistes of the Luiza metasedimentary Complex (**Fig.1**; *Delhal & Lamirant, 1979*). These metasedimentary rocks occur as isolated patches to the west of 23°E lying unconformably on the Archean to Paleoproterozoic Kanda-Kanda tonalites and granodiorite gneisses. To the east, the Archean to Paleoproterozoic craton was then marked by the Kibara (1.4–1.0 Ga) orogenic cycle (**Fig.1**; *Cahen et al., 1984; Johnson et al., 2005; De Waele and Fitzsimons, 2007; De Waele, 2008; Begg et al., 2009; Fernandez-Alonso et al., 2012*) occurring in Central Africa in Mesoproterozoic times during convergence between the Tanzania-Bangweulu Craton and the Congo-Kasai Craton. A plutonic activity is recorded around 1.3–1.4 Ga, poorly dated first between 1310 and 1350 Ma (*Cahen et al., 1974*). More recent compilations (*Tack et al., 2002; Kokonyangi et al., 2004; Tack et al., 2010*) restrict the Kibara tectono-magmatic event around 1.37–1.38 Ga (samples from the Kibara hills type-locality close to Mitwaba town).

U-Pb ages on detrital zircons obtained directly on sediments from the Mbuji-Mayi Supergroup, were analyzed by *Delpomdor et al., (2013)*. The youngest concordant grain is dated at  $1174 \pm 22$  Ma (Bld2 Formation in Kafuku drill core) and thus gives a maximum age around 1175 Ma for the sedimentation of the BI Group (**Fig.2**).

Three samples of galena, from the Lubi and Senga-Senga valleys and from the contact between BIIa and BIIb in Luembe valley (namely Kafuku) yielded conventional  $^{207}\text{Pb}/^{206}\text{Pb}$  ages of 910 Ma, 1040 Ma and 1065 Ma (*Cahen, 1954; Holmes and Cahen, 1955; Rauca, 1957*). Ages of 1040 and 1065 Ma have been attributed to syngenetic growth of galena and provide an age around 1055 Ma for the top of BI Group (Ble; *Cahen, 1974; Fig.2*).

Basaltic lavas topping the BII group at the confluence of the Mbuji-Mayi and Sankuru Rivers provided five nearly concordant K-Ar whole rock ages (*Cahen et al., 1974; 1984; Figs.1 & 2*) ranging from  $870 \pm 20$  Ma to  $953 \pm 20$  Ma. Among these, three results obtained on two samples were concordant:  $916 \pm 20$  Ma,  $942 \pm 20$  Ma, and  $953 \pm 20$  Ma. An estimated age of  $948 \pm 20$  Ma has been retained, corresponding to the two older ages. Note that the authors indicated that analyzes were carried out on altered samples and that no geochemical controls were used in the sample selection.

Moreover, studies of Mbuji-Mayi stromatolites by *Bertrand-Sarfati (1972)* compared to series in Mauritania suggested the deposition of the BII Group between around 1020 Ma and 910 Ma (isochrones by *Bonhomme & Clauer, 1972; Clauer, 1973*).

In the Lomami area (eastern part of the SMLL basin) an Ar-Ar dating on whole rock samples of dolerite sills gave an age of  $882.2 \pm 8.8$  Ma (*Delpomdor et al., 2013*). These dolerites were interpreted

as emplaced close to the contact between the BI and BII Groups and were attributed to the BI/BII limit by *Cahen et al. (1984)* and *Delpomdor et al. (2013, 2015)*. However, in the Lomami area, BI and BII were poorly studied (**Fig.1**) and no correlation with the Mbuji-Mayi area can be made. Thus, the stratigraphic position of these Lomami sills need to be confirmed in the field. They were not considered here since they are not directly related to our study.

#### 4. Sample description

To select appropriate lithologies, we observed and sampled the drill cores and also used the lithological descriptions of *Rauq (1957, 1970)* updated by *Delpomdor (2013)* and *Baludikay et al. (2016a)*. A total of 41 polished thin sections were cut through the five drill cores to study their petrology, microstructures (**Fig.3**) and to look for monazites, xenotimes and zircons with an optical microscope and a Scanning Electron Microprobe (**Fig.4**). Unfortunately, the BII Group samples contained no monazite nor xenotime. Only a few zircons were found, preventing a good geochronological statistic. In the BI Group samples, monazites, zircons and xenotimes were found in both Lubi and Kafuku drill cores (**Table 1**).

Samples of the BI Group consist of siliciclastic rocks composed of quartz, carbonates (mainly dolomite, ankerite and siderite), feldspars (K-feldspar and some plagioclase), oxides (anatase, hematite, goethite and lepidocrosite), sulphides (pyrite and marcassite), apatite and some phyllosilicates (white mica, biotite, chlorite and clay; **Fig.3**).

In the Lubi drill core, the lithostratigraphic succession (from bottom to top, *Delpomdor, 2013*) is as follows: BIb Subgroup consisting of dark conglomeratic sandstones and grey shaly limestones covered by alternations of dark micaceous sandstones and grey-pink brecciated dolomitic carbonated argillaceous sandstones; BIc (130 m) and BId Subgroups (100 m) exhibit micaceous sandstones with quartzites and sandstone in an argillaceous-carbonate matrix (BIc2 Formation, LU-69 & LU-60). Some gypsum and anhydrite veins are also observed in some samples (i.e. LU-60). BIE Subgroup (50 m) is composed of grey shaly dolomites and siltstones (BIE1 Formation, LU-149) below cherty dolomite layers. The uppermost BIE Subgroup (BIE2 Formation, 20 m) consists of grey cherty dolomites evolving to grey shaly dolomites and shales.

In the Kafuku drill core, the lithostratigraphic succession (from bottom to top, *Delpomdor, 2013*) is as follows: BId Subgroup (90 m) composed of pink sandstones and carbonated argillaceous sandstones (BId2 Formation, KA-95) and micaceous feldspathic pink quartzites with bedded micaceous sandstones (BId1 Formation, KA-97); BIE Subgroup (60 m) consists of micaceous shales evolving into argillaceous micaceous sandstones (BIE2 Formation, KA-80, KA-83 & KA-84), argillaceous dolomites and variegated shaly dolomites with gypsum veins, sandy pink and green or variegated zoned

micaceous sandstones with argillaceous or brecciated dolomites; B1e Subgroup (40 m) exhibits dark argillaceous or siliceous dolomites with shales and polygenic intraformational breccia, with cherty dolomites passing to dolomitic shaly pink limestones and breccias, micaceous sandstones or carbonated argillaceous sandstones; and the bottom of B11a Subgroup (10 m) composed of grey stromatolitic dolomites, micaceous pink quartzites and siliceous dolomites.

The observed xenotime minerals displayed different morphologies: rounded, well crystallized, between grains or in overgrowth around zircon (**Fig.7a**). Monazites were either rounded, very damaged or small and automorph (**Fig.7b**). They occasionally presented zoning. Zircons were very damaged and displayed oscillatory zoning (**Fig.7c**). A total of 37 monazite grains, 10 xenotime grains and 28 zircon grains were selected and dated.

## 5. Analytical methods

To better constrain the age of the diagenesis through the BI Group of the Mbuji-Mayi Supergroup, our research strategy is focused on different *in situ* technical approaches (i) U-Th-Pb chemical dating with Electron MicroProbe on monazites and xenotimes which are inherited and sometimes diagenetic (Montel *et al.*, 1996; McNaughton *et al.*, 1999; Rasmussen & Muhling, 2007) and (ii) U-Pb with Laser Ablation Inductively Coupled Plasma Mass Spectrometer (LA-ICP-MS) on inherited zircons, xenotimes and monazites.

### 5.1. U-Th-Pb chemical dating with Electron Microprobe

Electron Microprobe offers a high spatial resolution with a spot less than 1  $\mu\text{m}$  and is a non-destructive method capable to resolve a complex growth history of monazite (Suzuki *et al.*, 1994; Cocherie *et al.*, 1998; Williams *et al.*, 1999; Montel *et al.*, 1996, 2000; Crowley & Ghent, 1999; Terry *et al.*, 2000; Shaw *et al.*, 2001; Williams et Jercinovic, 2002; Goncalves *et al.*, 2004, 2005) but also of xenotime (Suzuki & Adachi, 1991; Griffin *et al.*, 2000; Asami *et al.*, 2002; Harrison *et al.*, 2002). This method also allows for mapping and for a pre-characterization of monazite and xenotime before isotopic analysis. Monazite contains negligible common Pb, only radiogenic Pb (Parrish, 1990), and is a robust geochronometer capable of recording multiple crystallization events including diagenesis in successive zoning around a core.

The theoretical basis for the method consists of measuring U- Th-Pb concentrations in a crystal and of calculating the age (t) by solving the equation:

$$Pb=(Th/232)*[exp(\lambda^{232}*t)-1]*208+(U/238.04)*0.9928*[exp(\lambda^{238}*t)-1]*206+(U/238.04)*0.0072*[exp(\lambda^{235}*t)-1]*207$$



where Pb, U, Th are in ppm, and  $\lambda^{232}$ ,  $\lambda^{235}$ ,  $\lambda^{238}$  are the radioactive decay constants of  $^{232}\text{Th}$ ,  $^{235}\text{U}$ , and  $^{238}\text{U}$ , respectively. Because monazite is rich in Th (commonly 3-15 wt%, sometime up to 25%) and U (a few hundreds of ppm up to 5%), radiogenic lead (Pb) accumulates very quickly, and in less than 100 million years reaches a level where a precise measurement can be performed with an electron microprobe.

The age calculated by this method has a geological meaning if: (1) non-radiogenic lead is negligible, and (2) no modification of the U/Th/Pb ratios has occurred except by radioactive decay. The validity of these hypotheses, was discussed by *Montel et al. (1994; 1996)* for monazite and by *Suzuki & Adachi (1991)*, *Griffin et al. (2000)*, *Asami et al. (2002)* and *Harrison et al. (2002)* for xenotime.

Errors and detection limits on Th, U and Pb are calculated using the statistical approach of *Ancey et al. (1978)*. Errors are given at  $\pm 2\sigma$  (with 95% confidence level; *Montel et al., 1996*, *Jercinovic & Williams, 2005*).

Analyzes were performed with a Cameca SX-Five electron microprobe equipped with five wavelength-dispersive spectrometers (WDS) at Camparis (UPMC, Paris). The operating conditions were 15 kV accelerating voltage and 100 nA beam current. The analyzed elements are: Si and P (K $\alpha$  line with a TAP monochromators), Ca (K $\alpha$  line with a PET monochromators), Y, La, Ce and Sm (L $\alpha$  line with a PET monochromators). Monazites and xenotimes can also contain Tb, Dy, Ho, Er, Tm, Yb, Lu, and F, which explain why the total (in % wt) is not equal to 100 in **Table 2**. However, these elements are not used to calculate the U-Th-Pb age. Four of the five available WDS were set with PET monochromators (two with a regular area, 22x32mm<sup>2</sup>, and two with a large area, 22x60mm<sup>2</sup>). They were operated simultaneously to analyze successively, U (M $\beta$  line), Th (M $\alpha$  line) and Pb (M $\beta$  line). Standards are ThO<sub>2</sub> for Th, UO<sub>2</sub> for U, PbS for Pb, Durango apatite for P and Ca, two rare earth doped glasses for Y, La, Ce and Sm and diopside for Si. The counting time was set at 20 s (peak + background) for all elements except U, Th and Pb for which 600 s was taken to reduce uncertainties. Measured ages are corrected using the reference monazite from Thompson Mine, Manitoba, Canada (TM, 1766 Ma). Maps are obtained using a focused beam in rastering mode, with a step size of 0.3  $\mu\text{m}$  and a dwell time of 250 ms per pixel.

## 5.2. U-Pb dating with LA-ICP-MS

U-Th-Pb geochronology of monazite, xenotime and zircon was conducted by Laser Ablation Inductively Coupled with Plasma Mass Spectrometry at the Laboratoire Magmas et Volcans, Clermont-Ferrand (France). The analyzes involve the ablation of minerals with a Resonetics Resolution M-50E powered by an ultra-short pulse ATL Atlex Excimer laser system operating at a wavelength of 193 nm. Spot diameters of 12  $\mu\text{m}$  (zircons) and 7  $\mu\text{m}$  (monazites and xenotimes) associated to repetition rates of 3 and 2 Hz with laser energy of 3 and 2.5 mJ were used respectively

for zircon and monazite/xenotime. The ablated material is carried into helium, and then mixed with nitrogen and argon, before injection into a plasma source of an Agilent 7500 cs ICP-MS equipped with a dual pumping system to enhance the sensitivity (Paquette *et al.*, 2014). The analytical method is basically similar to that developed by and reported in Paquette and Tiepolo (2007) and Hurai *et al.* (2010). The signals of  $^{204}\text{Pb} + \text{Hg}$ ,  $^{206}\text{Pb}$ ,  $^{207}\text{Pb}$ ,  $^{208}\text{Pb}$ ,  $^{232}\text{Th}$  and  $^{238}\text{U}$  masses are acquired. The occurrence of common Pb in the sample can be monitored by the evolution of the  $^{204}\text{Pb} + \text{Hg}$  signal intensity, but no common Pb correction was applied owing to the large isobaric interference from Hg. The  $^{235}\text{U}$  signal is calculated from  $^{238}\text{U}$  on the basis of the  $^{238}\text{U}/^{235}\text{U} = 137.88$ . Single analyzes consisted of 30 s of background integration with laser off followed by 1 min integration with the laser firing. Data are corrected for U–Pb and Th–Pb fractionation occurring during laser sampling and for instrumental mass discrimination (mass bias) by standard bracketing with repeated measurements of GJ-1 zircon (Jackson *et al.*, 2004) and Trebilcock monazite standards (Tomascak *et al.*, 1996). Data reduction was carried out with the software package GLITTER<sup>®</sup> (developed by the Macquarie Research Ltd.; Van Achterbergh *et al.*, 2001). For each analysis, the time-resolved signal of single isotopes and isotopic ratios was monitored and carefully inspected to verify the presence of perturbations related to inclusions, fractures, mixing of different age domains or common Pb. Calculated ratios were exported, and Concordia ages and diagrams were generated using the Isoplot/Ex v. 2.49 software package by Ludwig (2001). The analytical data are provided in **Tables 3 & 4** where errors are given at  $\pm 2\sigma$ . In the text and figures, all uncertainties in ages are given at the  $2\sigma$  level. The discordant data were considered only if they allowed possible Discordia lines to be defined on the Concordia diagrams; otherwise they were not taken into account because of doubtful interpretation. In laser-ablation ICPMS analyzes several factors that cannot be easily detected from the inspection of the time-resolved signals might contribute to discordance (e.g. common Pb, mixing of different age domains, small cracks or inclusions). The concentrations in U-Th-Pb were calibrated relative to the certified contents of GJ-1 zircon (Jackson *et al.*, 2004) and Trebilcock monazite standards (Tomascak *et al.*, 1996).

## 6. Results

### 6.1. Electron MicroProbe

A total of 6 monazites and 1 xenotime with a monazite inclusion (**Table 2; Fig.4**) were used for *in situ* EMP analyzes. Ages (corrected using a reference monazite) vary from 1039 to 1775 Ma. The youngest ages obtained on a small monazite (**Fig.4a**;  $15 \times 5 \mu\text{m}$ ), and on a xenotime (**Fig.4b**) from the Kafuku drill core were  $1051 \pm 138$  Ma and  $1039 \pm 219$  Ma respectively. This xenotime mineral shows different zonations and the younger age was only obtained in the external rim. The internal rim and a monazite inclusion are dated around 1150-1170 Ma, even if the errors are very large ( $2\sigma$ : 120 to 220

Myr). However these results are confirmed by the age obtained by LA-ICP-MS on the internal rim of xenotime at  $1217 \pm 68$  Ma (error is  $2\sigma$ ). To better constrain the ages of the external rims, we performed X-rays maps (Th  $M\alpha$ , Pb  $M\beta$  and U  $M\beta$ ) on 6 monazites from Lubi and Kafuku drill cores (**Figs.5 & 6**). We calculated a mean age and its associated error ( $1\sigma$ ; **Fig.5**) for 10 points of external rims of each monazite. Results clearly highlight that monazites display zonations with external rims between  $1049 \pm 29$  Ma and  $1061 \pm 20$  Ma. In **Fig.6**, two whole age populations (core vs rim) are graphically presented with a standard normal distribution presentation, corresponding to the pixel values from blue and green boxes respectively. Mean ages and their associated errors are calculated on the two age populations. Thus, the core mean age is around 1143–1152 Ma ( $n=120$ ) and the rim mean age is around 1040–1065 Ma ( $n=200$ ). This confirms results deduced from the **Figs.4 & 5** and results from *François et al. (2016)*.

## 6.2. LA-ICP-MS

### 6.2.1. Monazites and xenotimes

A total of 30 monazites and 9 xenotime are used for *in situ* U-Pb dating with LA-ICP-MS analyzes (**Table 3; Figs.7a,b & 8a**). Results provide  $^{207}\text{Pb}/^{206}\text{Pb}$  ages between 2783 and 1148 Ma for monazites and between 2151 and 1029 Ma for xenotimes. Three age groups stand out, the first between 1000 and 1700 Ma (74 % of monazites and xenotimes), the second between 1900 and 2400 Ma (20 %) and the third between 2700 and 2800 Ma (6 %). Only monazite grains have an age between 2300 and 2800 Ma. Overall, xenotimes are younger than monazites, and the youngest age occurs in a Kafuku xenotime crystal (**Figs.7a & 8a**). The Kafuku drill cores display a widest range of values; ages between 1900 and 2400 Ma are only recorded in this core as well as values below 1300 Ma (**Fig.8a**).

### 6.2.2. Zircons

A total of 28 zircons are used (**Table 4; Fig.8b**). They show a weak oscillatory zoning (**Fig.7c**) and a systematically high Th/U ratio (0.13–2.24) regardless of the variable amounts of U (36–1760 ppm) and Th (28–806 ppm) testifying inherited magmatic or metamorphic (for the low Th/U ratio) origins. Zircon ages obtained are highly discordant with a fan distribution and are poorly constrained, possibly because the system was reopened during the metamorphic and magmatic events. This highlights metamict zircons that lost radiogenic Pb and gained common Pb. Nevertheless, they provide  $^{207}\text{Pb}/^{206}\text{Pb}$  ages between 2911 and 1284 Ma (**Fig.6**). The youngest zircon yields a  $^{207}\text{Pb}/^{206}\text{Pb}$  apparent age at 1284 Ma and is located in Lubi drill core (**Fig.6**).

## 7. Discussion

### 7.1. Set of inherited ages

Our  $^{206}\text{Pb}/^{238}\text{U}$  zircon ages are highly discordant and no age trend is identified. Moreover,  $^{207}\text{Pb}/^{206}\text{Pb}$  ages are not significant due to the presence of common Pb. Given these results, we propose to perform a compilation of previous U-Pb geochronological studies in the region, and compare it with our ages. **Fig.9** summarizes previous U-Pb geochronological studies in the region from *Batumike et al. (2009; Fig.9a)*, *Delpomdor et al. (2013; Fig.9b)* and from this study (**Fig.9c**) together with a compilation of all these studies (**Fig.9d**). In *Batumike et al. (2009)*, 127 zircon grains were analyzed from the Luebo region (**Fig.9a**) close to rivers which cut through the Mbuji-Mayi Supergroup. Most of analyzes are concordant. The oldest zircon gives an age of  $3235 \pm 7$  Ma. Late- Archean zircons have ages ranging between 2903 and 2530 with two main populations grouped at  $2890 \pm 8$  Ma and  $2620 \pm 10$  Ma. Paleoproterozoic zircons show three populations at  $2390 \pm 20$ ,  $2150 \pm 5$  and  $2070 \pm 9$  Ma. Rare zircons have ages between 2000 and 1150 Ma, there is maybe a small population in the Mesoproterozoic at  $1441 \pm 17$  Ma ( $n = 4$ ) and  $1060 \pm 14$  Ma ( $n = 6$ ). There is a spread of ages from the Mesoproterozoic–Neoproterozoic transition to the end of the Neoproterozoic, with an important population observed around  $608 \pm 5$  Ma. Another age group is observed at 493 Ma ( $n = 14$ ). In the second study (*Delpomdor et al., 2013*), 355 zircon grains were analyzed from siliciclastic rocks belonging to the BI Group in two samples from Kafuku drill core (RG41375, Bld2 and RG41382, Bld2), and in two samples from Lubi drill core (RG57673, Bld2 and RG57809, Bld1). 165 of 336 analyzes are concordant and used for the probability plot (**Fig.9b**). Three main peaks are highlighted between *ca.* 1.1 and 1.4 Ga, 1.7 and 2.1 Ga, and 2.7 and 2.9 Ga.

Our dating is concordant with these previous studies (**Fig.9c & d**) albeit less of data and except without ages older than 3.0 Ga and younger than 1.0 Ga, and allow to define the different origin of the sediments constituting the lower part of the Mbuji-Mayi Supergroup:

- (i) ages between 2.6 and 2.8 Ga correspond to the age of intrusion of Dibaya granitic and migmatitic Complex (Northern part of Congo-Kasai Craton) and are compatible with results of *Delhal et al. (1975)*, *Cahen et al. (1984)* and *Delpomdor et al. (2013)*.
- (ii) ages between 1.9 and 2.4 Ga are scattered but consistent with the Luiza metasedimentary Complex (*Ledent et al., 1962; Delhal & Ledent, 1973; Delhal & Ladmirant, 1979; Cahen et al. 1984*), where a thermo-tectonic event is recorded between 2.0 and 2.2 Ga (Rb-Sr on micas from granites and pegmatites; *Delhal & Ledent, 1973*). It could be also consistent with the Lulua Complex, probably older than  $1468 \pm 30$  Ma (*Snelling, unpublished data*) and around 2.0–2.2 Ga (K-Ar; *Delhal & Ladmirant., 1979*).
- (iii) the age peak around 1.8–1.9 Ga corresponds to a system of Palaeoproterozoic belts, respectively on the southeastern margin of the Tanzania Craton (Usagara Belt), and between the Bangweulu Block and Tanzania Craton (Ubende Belt; *de Waele et al., 2008*). It results from an important tectonothermal event during the amalgamation of the

Tanzania Craton and the Bangweulu Block (*Lenoir et al., 1994; Möller et al., 1995; Boven et al., 1999; Reddy et al., 2003; Collins et al., 2004; Sommer et al., 2005*).

- (i) ages between 1.1 and 1.7 Ga are coeval with the Kibara orogenic cycle occurring during convergence between the Tanzania-Bangweulu Craton and the Congo-Kasai Craton (*Cahen et al., 1984; De Waele, 2004; Johnson et al., 2005; De Waele and Fitzsimons, 2007; Begg et al., 2009; Fernandez-Alonso et al., 2012*), with a plutonic activity peak at 1.3–1.4 Ga (*Tack et al., 2002; Kokonyangi et al., 2004, 2006, 2007; Tack et al., 2010*).

Archean ages between 2.6 and 2.8 Ga are clearly recorded in the Lubi samples (**Fig.9b-d & Fig.10c** in green) and in the Luebo region (**Fig.9a, d & Fig.10b** in yellow) due to the proximity with the Dibaya Complex (**Fig.10a**). The Ubende/Usagara (1.8–1.9 Ga) and Kibara (1.1–1.7 Ga) ages are preferentially found in the Kafuku samples (**Fig.9b, c & Fig.10d** in purple) located in the southeastern part of the Mbuji-Mayi area (**Fig.10a**). The quasi-absence of zircons with ages of 1.8–1.9 Ga and 1.3–1.4 Ga in the Luebo region (**Fig.10b**) clearly indicates that these zircons did not come from the eastern margin, where rocks of these ages (Paleoproterozoic Bangweulu Block and Mesoproterozoic Kibara Belt) are known (*Batumike et al., 2009*).

Furthermore, the source of sediments has changed over time within the Lubi and the Kafuku drill cores (**Fig.11**). In the Lubi drill core, we observe a probable unique Archean Congo-Kasai source in the Blc1 Formation followed by a dominantly Kibara source in the Blc2 Formation, and again Archean and Kibara sources with minor Usagara and Ubende contributions in the Bld2 Formation. The sediments increasingly come from a remote easterly source, more than 400 km away. Also, an important supply of sediments in the Ble1 Formation came from the Lulua and Luiza complexes while the proportion of sediments from the Kibara Belt was strongly decreasing. In the Kafuku drill core, the Bld1 Formation was marked by a probable Kibara supply, while the Bld2 Formation deposit (Lower and Upper) recorded also an important Usagara and Ubende source with minor Congo-Kasai source. The BIE2 Formation showed, with an Archean, a Usagara/Ubende and a Kibara sources, also a contribution from the Lulua and Luiza complexes. This was probably due to the hiatus of the BIE in the Lubi drill core and a more distant sediment supply from the WSW (**Fig.10a**). Thus, sediments from the Mbuji-Mayi area indicate a multiple provenance from the Dibaya Complex/Congo-Kasai Craton and from the network of belts to the east/southeast (**Fig.10**). These dating highlight a complex provenance for sediments composing the BI Group with poly-magmatic and -metamorphic origins. This also testifies, between Lubi and Kafuku, the presence of natural barriers at the boundary between the continent and the sedimentary basin which temporarily blocked the supply of sediments from a given source.

## 7.2. Diagenesis of Mbuji-Mayi Supergroup

U-Pb ages obtained on sediment from the Mbuji-Mayi Supergroup by *Delpomdor et al. (2013)* suggest a maximum age at 1175 Ma for the beginning of BI Group diagenesis. Our results with EMP on the Kafuku and Lubi drill cores clearly highlight younger ages (between 1039 and 1065 Ma; **Figs. 4-6 & 11**) obtain on external rims of monazites and xenotimes, probably corresponding to a recrystallization during diagenesis. These results are confirmed with  $^{207}\text{Pb}/^{206}\text{Pb}$  age at 1029 Ma obtain on a xenotime with LA-ICP-MS (**Figs. 7a & 8a**). Thus, we propose a diagenesis of BI Group younger than 1175 Ma and probably around 1030-1065 Ma. This confirms previous Pb-Pb ages obtained on syngenetic galena around 1055 Ma (BI Group; *Cahen, 1954; Holmes and Cahen, 1955; Raucq, 1957*) and correlation of *Bertrand-Sarfati (1972)* with series of Mauritania dating the BI Group deposit, overlying the BI Group, between  $1019 \pm 36$  Ma and  $909 \pm 37$  Ma (isochron ages by *Bonhomme & Clauer, 1972; Clauer, 1973*). Dating on basaltic pillow lavas topping the Mbuji-Mayi Supergroup (*Cahen et al., 1974 and Cahen et al., 1984*) limit in time the end of sedimentary deposit of this Supergroup before 950 Ma. Moreover, the exceptionally diverse and well-preserved organic-walled microfossil assemblage from the Mbuji-Mayi Supergroup and comparison with other worldwide microfossil assemblages shows that the Mbuji-Mayi assemblage is likely Late Mesoproterozoic–Early Neoproterozoic (*Baludikay et al., 2016a*), consistent also with our geochronological data.

### 7.3. Implications for eukaryotic diversification in Central Africa

Proterozoic microfossils constitute a major source of paleontological information essential for understanding early life evolution. In particular, they document the evolution of biological innovations and patterns of diversification of early eukaryotes (e.g. *Butterfield, 2015; Javaux, 2011; Javaux & Knoll, 2016; Knoll, 2014*). Eukaryotic cells appeared at least 1.7 Ga ago but their diversification increased around 1.2-0.8 Ga (e.g. *Knoll, 1992; Xiao et al., 1997; Butterfield, 2000, 2004; Javaux et al., 2003, 2004; Javaux, 2011; Porter et al., 2003*; for an alternative view see *Cavalier-Smith, 2002*). *Baludikay et al. (2016a)* recently described an exquisitely preserved assemblage of organic-walled microfossils in the Mbuji-Mayi Supergroup, and documented for the first time the diversification of early eukaryotes in Central Africa, similarly to other worldwide assemblages in the Late Mesoproterozoic–Early Neoproterozoic (e.g. *Beghin et al., 2017*). Africa in general had a poorly documented Proterozoic microfossil record, but recent studies (*Baludikay et al., 2016a; Beghin et al., 2017*) reported exquisitely preserved assemblages providing accurate dating of the DRC succession is thus of prime importance to better constrain the patterns of early biosphere evolution in Africa and worldwide.

## 8. Conclusions



This study provides new time constraints for the diagenesis and sediment sources from the lower part of the Mbuji-Mayi Supergroup. The beginning of the BI Group diagenesis is estimated around 1065 Ma while the end is probably around 1030 Ma. We note variations of deposition regime (carbonated vs siliciclastic) and supply of sediments between the different drill cores with diverse terrigenous contributions, coming occasionally from more than 100's km away. This study also contributes to date microfossil levels and to the characterization of their paleoenvironments. Our results are consistent with biostratigraphic data from *Baludikay et al. (2016a)* supporting the occurrence of worldwide changes around the Mesoproterozoic/Neoproterozoic boundary. We significantly improve the constraints on the timing of early eukaryotes diversification, thereby contributing to a better understanding of early biosphere evolution, preserved in the Democratic Republic of Congo rock record and more broadly in the understudied Proterozoic African deposits.

### 9. Acknowledgements

We thank the Royal Museum for Central Africa (RMAC, Tervuren/Belgium) for access to the drill cores for sampling, Omar Boudouma (UPMC, Paris) and Philippe Compère (ULg) for SEM imagery. This paper has benefited from discussions with Max Fernandez-Alonso from RMAC and constructive reviews from Damien Delvaux and an anonymous reviewer helping to significantly improve the manuscript.

Research funding came from the European Research Council Stg ELITE FP7/308074, the BELSPO IAP PLANET TOPERS and the Francqui Foundation. This work was also supported by a STSM Grant (ORIGINS COST Action TD1308) for ICP-MS analyzes.

### 10. References

- Ancey, M., Bastenaire, F., & Tixier, R. (1978). Application des méthodes statistiques en microanalyse. *Microanalyse, microscopie électronique à balayage*, 323-347.
- Asami, M., Suzuki, K., & Grew, E. S. (2002). Chemical Th-U-total Pb dating by electron microprobe analysis of monazite, xenotime and zircon from the Archean Napier Complex, East Antarctica: evidence for ultra-high-temperature metamorphism at 2400 Ma. *Precambrian Research*, 114(3), 249–275.
- Baludikay, B. K., Storme, J.-Y., François, C., Baudet, D., & Javaux, E. J. (2016a). A diverse and exquisitely preserved organic-walled microfossil assemblage from the Meso-Neoproterozoic Mbuji-Mayi Supergroup (Democratic Republic of Congo) and implications for Proterozoic biostratigraphy. *Precambrian Research*, 281, 166-184.
- Baludikay, B. K., Storme, J.-Y., Baudet, D., François, C., & Javaux, E. (2016b). Thermal maturation of carbonaceous material from Mbuji-Mayi Supergroup (Kasai, Democratic Republic of Congo). *Geophysical Research Abstract*, Vol. 18, EGU2016-4574.
- Batumike, J. M., Griffin, W. L., O'Reilly, S. Y., Belousova, E. A., & Pawlitschek, M. (2009). Crustal evolution in the central Congo-Kasai Craton, Luebo, DR Congo: insights from zircon U-Pb ages, Hf-isotope and trace-element data. *Precambrian Research*, 170(1), 107–115.
- Begg, G. C., Griffin, W. L., Natapov, L. M., O'Reilly, S. Y., Grand, S. P., O'Neill, C. J., Hronsky, J. M. A., Poudjom Djomani, Y., Swain, C. J., Deen, T., & Bowden, P. (2009). The lithospheric architecture of Africa: Seismic tomography, mantle petrology, and tectonic evolution. *Geosphere*, 5(1), 23–50.

- Beghin J., Storme JY, Houzay JP, Blanpied C, Gueneli N, Brocks JJ, Poulton SW & Javaux EJ (2017). Microfossils from the Late Mesoproterozoic (1.1 Ga) Atar/El Mreïti Groups, Taoudeni Basin, Mauritania, Northwestern Africa. *Precambrian research*, 291, 63-82.
- Bertrand-Sarfati, J. (1972). *Stromatolites colonnaires du Précambrien supérieur du Sahara nord-occidental: inventaire, morphologie et microstructure des laminations, corrélations stratigraphiques*. Éditions du Centre national de la recherche scientifique.
- Bonhomme, M., & Clauer, N. (1972). Possibilités d'utilisation stratigraphique des datations directes rubidium-strontium sur les minéraux et les roches sédimentaires. *Mém. Bur. Rech. Géol. Min*, 77, 943-950.
- Boven, A., Theunissen, K., Sklyarov, E., Klerkx, J., Melnikov, A., Mruma, A., & Punzalan, L. (1999). Timing of exhumation of a high-pressure mafic granulite terrane of the Paleoproterozoic Ubende belt (West Tanzania). *Precambrian Research*, 93(1), 119-137.
- Butterfield, N. J. (2000). Bangiomorpha pubescens n. gen., n. sp.: implications for the evolution of sex, multicellularity, and the Mesoproterozoic/Neoproterozoic radiation of eukaryotes. *Paleobiology*, 26(3), 386-404.
- Butterfield, N. J. (2004). A vaucheriacean alga from the middle Neoproterozoic of Spitsbergen: implications for the evolution of Proterozoic eukaryotes and the Cambrian explosion. *Paleobiology*, 30(02), 231-252.
- Butterfield, N. J. (2015). Early evolution of the Eukaryota. *Palaeontology*, 58(1), 5-17.
- Cahen, L. (1954). Résultats géochronologiques obtenus sur des minéraux du Congo jusqu'en Mai 1954. *Bulletin de La Société Géologique de Belgique*, 77, B268-B281.
- Cahen, L. (1972). L'Ouraninite de 620 ma post-date tout le Katangien, mise au point. *Mus. roy. Afr. centr. Dept. Géol. Minér., Rapp. Ann*, 35-38.
- Cahen, L. (1974). Geological background to the copper-bearing strata of southern Shaba (Zaire). *Annales de La Société Géologique de Belgique*, 57-77.
- Cahen, L., Ledent, D., & Snelling, N. J. (1974). Données géochronologiques dans le Katangien inférieur du Kasai oriental et du Shaba nord-oriental (République du Zaïre). *Mus. Roy. Afr. Centr.-Tervuren (Belg.) Dépt. Geol. Min. Rapport Annuel*, 1974, 51-70.
- Cahen, L., Snelling, N. J., Delhal, J., Vail, J. R., Bonhomme, M., & Ledent, D. (1984). The geochronology and evolution of Africa. Clarendon. Oxford.
- Cavalier-Smith, T. (2002). The phagotrophic origin of eukaryotes and phylogenetic classification of Protozoa. *International Journal of Systematic and Evolutionary Microbiology*, 52(2), 297-354.
- Clauer, N. (1973). Utilisation de la méthode rubidium-strontium pour la datation de niveaux sédimentaires du Précambrien supérieur de l'Adrar mauritanien (Sahara occidental) et la mise en évidence de transformations précoces des minéraux argileux. *Geochimica et Cosmochimica Acta*, 37(10), 2243-2255.
- Cocherie, A., Legendre, O., Peucat, J. J., & Kouamelan, A. N. (1998). Geochronology of polygenetic monazites constrained by in situ electron microprobe Th-U-total lead determination: implications for lead behaviour in monazite. *Geochimica et Cosmochimica Acta*, 62(14), 2475-2497.
- Collins, A. S., Reddy, S. M., Buchan, C., & Mruma, A. (2004). Temporal constraints on Palaeoproterozoic eclogite formation and exhumation (Usagaran Orogen, Tanzania). *Earth and Planetary Science Letters*, 224(1), 175-192.



- Crowley, J. L., & Ghent, E. D. (1999). An electron microprobe study of the U-Th-Pb systematics of metamorphosed monazite: the role of Pb diffusion versus overgrowth and recrystallization. *Chemical Geology*, 157(3), 285–302.
- De Waele, B. (2004). The Proterozoic geological history of the Irumide belt, Zambia. *Unpublished MSc Thesis, Curtin University of Technology, Australia*.
- De Waele, B., & Fitzsimons, I. C. W. (2007). The nature and timing of Palaeoproterozoic sedimentation at the southeastern margin of the Congo Craton; zircon U-Pb geochronology of plutonic, volcanic and clastic units in northern Zambia. *Precambrian Research*, 159(1), 95–116.
- De Waele, B., Johnson, S. P., & Pisarevsky, S. A. (2008). Palaeoproterozoic to Neoproterozoic growth and evolution of the eastern Congo Craton: its role in the Rodinia puzzle. *Precambrian Research*, 160(1), 127–141.
- Delhal, J., & Ledent, D. (1973). L'âge du complexe métasédimentaire de Luiza, région du Kasai, Zaïre. *Ann. Soc. Géol. Belg*, 96, 289–300.
- Delhal, J. & Ladmirant, H. (1979). *Carte géologique à l'échelle du 1/200.000, Notice explicative de la feuille Mbuji-Mayi (Degré carré S7/23)* (Service géologique, bureau de Kinshasa).
- Delhal, J., Ledent, D. & Pasteels P. (1975). L'âge du complexe granitique et migmatitique de Dibaya (Région du Kasai, Zaïre) par les méthodes Rb-Sr et U-Pb. *Ann. Soc. Géol. Belg*, 98, 141-154.
- Delhal, J., Ledent, D., & Torquato, J. R. (1976). Nouvelles données géochronologiques relatives au complexe gabbro-noritique et charnockitique du bouclier du Kasai et à son prolongement en Angola. *Ann. Soc. Géol. Belg*, 99, 211-226.
- Delpomdor, F. (2013). Lithostratigraphie et sédimentologie de la chaîne Ouest Congolienne du Néoprotérozoïque supérieur (Formation de la Diamictite supérieure et Sous-groupe du Schisto-Calcaire) Bas-Congo, République Démocratique du Congo. *Unpublished MSc Thesis, Université Libre de Bruxelles, Belgium*.
- Delpomdor, F., Blanpied, C., Virgone, A., & Prétat, A. (2015). Sedimentology and Sequence Stratigraphy of the Late Precambrian Carbonates of the Mbuji-Mayi Supergroup in the Sankuru-Mbuji-Mayi-Lomami-Lovoy Basin (Democratic Republic of the Congo). In *Geology and Resource Potential of the Congo Basin* (pp. 59–76). Springer.
- Delpomdor, F., Linnemann, U., Boven, A., Gärtner, A., Travin, A., Blanpied, C., Prétat, A. (2013). Depositional age, provenance, and tectonic and paleoclimatic settings of the late Mesoproterozoic-middle Neoproterozoic Mbuji-Mayi Supergroup, Democratic Republic of Congo. *Palaeogeography, Palaeoclimatology, Palaeoecology*, 389, 4–34.
- Fernandez-Alonso, M., Cutten, H., De Waele, B., Tack, L., Tahon, A., Baudet, D., & Barritt, S. D. (2012). The Mesoproterozoic Karagwe-Ankole Belt (formerly the NE Kibara Belt): The result of prolonged extensional intracratonic basin development punctuated by two short-lived far-field compressional events. *Precambrian Research*, 216, 63–86.
- François, C., Kabamba Baludikay, B., Storme, J.-Y., Baudet, D., Paquette, J.-L., Fialin, M., Javaux, E. (2016). New geochronological history of the Mbuji-Mayi Supergroup (Proterozoic, DRC) through U-Pb and Sm-Nd dating. *Geophysical Research Abstract*, Vol. 18, EGU2016-6405.
- Goncalves, P., Nicollet, C., & Montel, J.-M. (2004). Petrology and in situ U-Th-Pb monazite geochronology of ultrahigh-temperature metamorphism from the Andriamena mafic unit, north-central Madagascar. Significance of a petrographical P-T path in a polymetamorphic context. *Journal of Petrology*, 45(10), 1923–1957.

- Goncalves, P., Williams, M. L., & Jercinovic, M. J. (2005). Electron-microprobe age mapping of monazite. *American Mineralogist*, 90(4), 578–585.
- Griffin, B. J., Forbes, D., & McNaughton, N. J. (2000). An Evaluation of Dating of Diagenetic Xenotime by Electron Microprobe. *MICROSCOPY AND MICROANALYSIS-NEW YORK*-, 6(2), 408–409.
- Harrison, T. M., Catlos, E. J., & Montel, J.-M. (2002). U-Th-Pb dating of phosphate minerals. *Reviews in Mineralogy and Geochemistry*, 48(1), 524–558.
- Hurai, V., Paquette, J.L., Huraiová, M. & Konečný, P., (2010). Age of deep crustal magmatic chambers in the intra-Carpathian back-arc basin inferred from LA-ICPMS U-Th-Pb dating of zircon and monazite from igneous xenoliths in alkali basalts. *J. Volc. Geo. Res.*198, 275-287.
- Holmes, A., & Cahen, L. (1955). African geochronology. *Colonial Geology and Mineral Resources* 5 (1), 3–38.
- Jackson, S. E., Pearson, N. J., Griffin, W. L., & Belousova, E. A. (2004). The application of laser ablation-inductively coupled plasma-mass spectrometry to in situ U-Pb zircon geochronology. *Chemical Geology*, 211(1), 47–69.
- Javaux, E. (2011). Early eukaryotes in Precambrian oceans. *Origins and Evolution of Life: An Astrobiological Perspective*, 414–449.
- Javaux, E. J., Knoll, A. H., & Walter, M. (2003). Recognizing and interpreting the fossils of early eukaryotes. *Origins of Life and Evolution of the Biosphere*, 33(1), 75–94.
- Javaux, E. J., Knoll, A. H., & Walter, M. R. (2004). TEM evidence for eukaryotic diversity in mid-Proterozoic oceans. *Geobiology*, 2(3), 121–132.
- Javaux EJ, and Knoll AH (2016) Micropaleontology of the lower Mesoproterozoic Roper Group, Australia and implications for early eukaryote evolution. *Journal of Paleontology*, 91(2), 199-229.
- Jercinovic, M. J., & Williams, M. L. (2005). Analytical perils (and progress) in electron microprobe trace element analysis applied to geochronology: Background acquisition, interferences, and beam irradiation effects. *American Mineralogist*, 90(4), 526-546.
- Johnson, S. P., Rivers, T., & De Waele, B. (2005). A review of the Mesoproterozoic to early Palaeozoic magmatic and tectonothermal history of south-central Africa: implications for Rodinia and Gondwana. *Journal of the Geological Society*, 162(3), 433–450.
- Kadima, E., Delvaux, D., Sebagenzi, S. N., Tack, L., & Kabeya, S. M. (2011). Structure and geological history of the Congo Basin: an integrated interpretation of gravity, magnetic and reflection seismic data. *Basin Research*, 23(5), 499–527.
- Knoll, A. H. (1992). The early evolution of eukaryotes: a geological perspective. *Science*, 256(5057), 622.
- Knoll, A. H. (2014). Paleobiological perspectives on early eukaryotic evolution. *Cold Spring Harbor Perspectives in Biology*, 6(1), a016121.
- Kokonyangi, J., Armstrong, R., Kampunzu, A. B., Yoshida, M., & Okudaira, T. (2004). U-Pb zircon geochronology and petrology of granitoids from Mitwaba (Katanga, Congo): implications for the evolution of the Mesoproterozoic Kibaran belt. *Precambrian Research*, 132(1), 79–106.
- Kokonyangi, J. W., Kampunzu, A. B., Armstrong, R., Arima, M., Yoshida, M., & Okudaira, T. (2007). U-Pb SHRIMP Dating of Detrital Zircons from the Nzilo Group (Kibaran Belt): Implications for the Source of Sediments and Mesoproterozoic Evolution of Central Africa. *The Journal of Geology*, 115(1), 99–113.

- Kokonyangi, J. W., Kampunzu, A. B., Armstrong, R., Yoshida, M., Okudaira, T., Arima, M., & Ngulube, D. A. (2006). The Mesoproterozoic Kibari belt (Katanga, SE DR Congo). *Journal of African Earth Sciences*, 46(1), 1–35.
- Lenoir, J. L., Liégeois, J.-P., Theunissen, K., & Klerkx, J. (1994). The Palaeoproterozoic Ubendian shear belt in Tanzania: geochronology and structure. *Journal of African Earth Sciences*, 19(3), 169–184.
- Ludwig, K. L. (2001). Using Isoplot/EX, v2. 49, a geochronological toolkit for Microsoft Excel. *Berkeley Geochronological Center Special Publication*.
- McNaughton, N. J., Rasmussen, B., & Fletcher, I. R. (1999). SHRIMP uranium-lead dating of diagenetic xenotime in siliciclastic sedimentary rocks. *Science*, 285(5424), 78–80.
- Möller, A., Appel, P., Mezger, K., & Schenk, V. (1995). Evidence for a 2 Ga subduction zone: eclogites in the Usagaran belt of Tanzania. *Geology*, 23(12), 1067–1070.
- Montel, J. M., Kornprobst, J., & Vielzeuf, D. (2000). Preservation of old U-Th-Pb ages in shielded monazite: example from the Beni Bousera Hercynian kinzigites (Morocco). *Journal of Metamorphic Geology*, 18(3), 335–342.
- Montel, J.-M., Foret, S., Veschambre, M., Nicollet, C., & Provost, A. (1996). Electron microprobe dating of monazite. *Chemical Geology*, 131(1), 37–53.
- Paquette, J.-L., & Tiepolo, M. (2007). High resolution (5  $\mu\text{m}$ ) U-Th-Pb isotope dating of monazite with excimer laser ablation (ELA)-ICPMS. *Chemical Geology*, 240(3), 222–237.
- Paquette, J.L., Piro, J.L., Devidal, J.L., Bosse, V. & Didier, A. (2014) Sensitivity enhancement in LA-ICP-MS by N<sub>2</sub> addition to carrier gas: application to radiometric dating of U-Th-bearing minerals. *Agilent ICP-MS journal*, 58, 4-5.
- Parrish, R. R. (1990). U-Pb dating of monazite and its application to geological problems. *Canadian Journal of Earth Sciences*, 27(11), 1431–1450.
- Porter, S. M., Meisterfeld, R., & Knoll, A. H. (2003). Vase-shaped microfossils from the Neoproterozoic Chuar Group, Grand Canyon: a classification guided by modern testate amoebae. *Journal of Paleontology*, 77(03), 409–429.
- Rasmussen, B., & Muhling, J. R. (2007). Monazite begets monazite: evidence for dissolution of detrital monazite and reprecipitation of syntectonic monazite during low-grade regional metamorphism. *Contributions to Mineralogy and Petrology*, 154(6), 675–689.
- Raucq, P. (1957). Contribution à la connaissance du Système de la Bushimay. *Annales Du Musée Royal Du Congo Belge (Tervuren)*, 8(18), 427.
- Raucq, P. (1970). Nouvelles acquisitions sur le système de la Bushimay. *Annales/Musee de l'Afrique Centrale. Sciences Geologiques*, 8(69).
- Reddy, S. M., Collins, A. S., & Mruma, A. (2003). Complex high-strain deformation in the Usagaran Orogen, Tanzania: structural setting of Palaeoproterozoic eclogites. *Tectonophysics*, 375(1), 101–123.
- Shaw, C. A., Karlstrom, K. E., Williams, M. L., Jercinovic, M. J., & McCoy, A. M. (2001). Electron-microprobe monazite dating of ca. 1.71-1.63 Ga and ca. 1.45-1.38 Ga deformation in the Homestake shear zone, Colorado: Origin and early evolution of a persistent intracontinental tectonic zone. *Geology*, 29(8), 739–742.

- Sommer, H., Kröner, A., Muhongo, S., & Hauzenberger, C. (2005). SHRIMP zircon ages for post-Usagaran granitoid and rhyolitic rocks from the Palaeoproterozoic terrain of southwestern Tanzania. *South African Journal of Geology*, 108(2), 247–256.
- Suzuki, K., & Adachi, M. (1991). Precambrian provenance and Silurian metamorphism of the Tsubonosawa paragneiss in the South Kitakami terrane, Northeast Japan, revealed by the chemical Th-U-total Pb isochron ages of monazite, zircon and xenotime. *Geochemical Journal*, 25(5), 357–376.
- Suzuki, K., & Adachi, M. (1994). Middle Precambrian detrital monazite and zircon from the Hida gneiss on Oki-Dogo Island, Japan: their origin and implications for the correlation of basement gneiss of Southwest Japan and Korea. *Tectonophysics*, 235(3), 277–292.
- Tack, L., Baudet, D., Chartry, G., Deblond, A., Fernandez-Alonso, M., Lavreau, J., others. (2002). The Northeastern Kibaran Belt (NKB) reconsidered: evidence for a c. 1370 Ma-old, repeatedly reactivated Kibara mobile belt, preceding the c. 1.0 Ga Rodinia Supercontinent assembly. In *19th Colloquium of African Geology, El Jadida, Morocco* (pp. 19–23).
- Tack, L., Wingate, M. T. D., De Waele, B., Meert, J., Belousova, E., Griffin, B., Fernandez-Alonso, M. (2010). The 1375Ma “Kibaran event” in Central Africa: Prominent emplacement of bimodal magmatism under extensional regime. *Precambrian Research*, 180(1), 63–84.
- Terry, M. P., Robinson, P., Hamilton, A., & Jercinovic, M. J. (2000). Monazite geochronology of UHP and HP metamorphism, deformation, and exhumation, Nordøyane, Western Gneiss Region, Norway. *American Mineralogist*, 85(11-12), 1651–1664.
- Tomascak, P. B., Krogstad, E. J., & Walker, R. J. (1996). U-Pb monazite geochronology of granitic rocks from Maine: implications for late Paleozoic tectonics in the northern Appalachians. *The Journal of Geology*, 104(2), 185-195.
- Van Achterbergh, E., Ryan, C. G., Jackson, S. E., & Griffin, W. L. (2001). Data reduction software for LA-ICP-MS. *Laser-Ablation-ICPMS in the Earth Sciences—principles and Applications. Miner Assoc Can (short Course Series)*, 29, 239–243.
- Wazilewski, I. (1953). Exploration en profondeur des formations du Système de la Bushimay (Bakwanga, Kasai, Congo Belge). Université de Louvain.
- Williams, M. L., & Jercinovic, M. J. (2002). Microprobe monazite geochronology: putting absolute time into microstructural analysis. *Journal of Structural Geology*, 24(6), 1013–1028.
- Williams, M. L., Jercinovic, M. J., & Terry, M. P. (1999). Age mapping and dating of monazite on the electron microprobe: Deconvoluting multistage tectonic histories. *Geology*, 27(11), 1023–1026.
- Xiao, S., Knoll, A. H., Kaufman, A. J., Yin, L., & Zhang, Y. (1997). Neoproterozoic fossils in Mesoproterozoic rocks? Chemostratigraphic resolution of a biostratigraphic conundrum from the North China Platform. *Precambrian Research*, 84(3), 197–220.

## 11. Captions

**Fig.1.** Geological map of the Sankuru-Mbuji-Mayi-Lomami-Lovoy (SMLL) basin. Drill cores: LU: Lubi, KN: Kanshi, BK: Bena Kalenda, BT: Bena Tshovu and Ka: Kafuku. Age data from Cahen *et al.* (1954, 1972, 1984), Cahen (1974), Holmes & Cahen (1955) and Delpomdor *et al.* (2013). Map modified after Delpomdor *et al.* (2013).

**Fig.2.** Stratigraphy of the Mbuji-Mayi area. Ages from (a) Delhal *et al.* (1975), (b) Cahen *et al.* (1984), (c) Delpomdor *et al.* (2013), (d) Cahen *et al.* (1954), (e) Holmes & Cahen (1955), (f) Cahen *et al.* (1972) and (g) Cahen (1974). Log modified from Raucq (1957, 1970) and Baludikay *et al.* (2016a).

**Fig.3.** Photomicrographs of (a) sample LU-149: siltstone with feldspar, quartz and white mica, (b) sample LU-69: mudstone with feldspar, quartz, biotite, chlorite, white mica, apatite and barite, (c) sample LU-60: siltstone composed of quartz, feldspar, white mica, biotite and chlorite with large fractures of gypsum, anhydrite and celestite, (d) sample KA-80: sandstone showing flakes of clay minerals in a matrix of quartz, feldspar and white micas, (e) sample KA-83: argillaceous siltstone with quartz, feldspar, carbonate, biotite, chlorite and oxide, (f) sample KA-84: shaly dolomite with feldspar, quartz and dolomite megacrysts, (g) sample KA-95: carbonated argillaceous sandstone with quartz, mica, oxide, clay and carbonate and (h) sample KA-97: micaceous sandstones with feldspar, quartz, biotite, chlorite and oxide.

**Fig.4.** Backscattered image for (a) monazite (KA-95) and (b) xenotime with monazite inclusion (KA-97) in Kafuku drill core with location and age of EMP analyzes (errors are  $2\sigma$ ). Dashed white circle in (b) represent size of the the LA-ICP-MS  $^{207}\text{Pb}/^{206}\text{Pb}$  spot analysis (error is  $2\sigma$ ).

**Fig.5.** Backscattered images and X-ray maps (Th M $\alpha$ , Pb M $\beta$  and U M $\beta$ ) for four monazites from Kafuku drill core (a & b) from KA-84 sample and (c & d) from KA-98 sample. Blue spots represent location of EMP analyzes for rims of the different monazites (spots are magnified 6 times for better viewing). Corresponding ages are in tables on the right with corresponding mean age and standard deviation ( $1\sigma$ ).

**Fig.6.** Backscattered images and X-ray maps (Th M $\alpha$ , Pb M $\beta$  and U M $\beta$ ) for two monazites from Lubi drill core and corresponding ages calculated (standard normal distribution of the pixel values from the green and blue areas), showing two distinct age domains, in core (in green) and in rims (in blue) respectively.

**Fig.7.** Backscattered electron imaging of some (a) xenotimes on the left column, (b) monazites on the middle column and (c) zircons on the right column of selected samples from the Kafuku and Lubi drill cores. Circles show location and age (Ma) of LA-ICP-MS  $^{207}\text{Pb}/^{206}\text{Pb}$  spot analyzes. Scale bar is 10  $\mu\text{m}$ .

**Fig.8.** Concordia diagrams for LA-ICP-MS U-Th-Pb analyzes on (a) 30 monazite and 9 xenotime grains (43 and 18 analyzes respectively) with inset between 900 and 1500 Ma and (b) 28 zircons (40 analyzes, dotted ellipses represent analyzes with a concordance lower than 70%). Error ellipses are  $2\sigma$ .

**Fig.9.**  $^{207}\text{Pb}/^{206}\text{Pb}$  apparent ages (Ga) on (a) zircons from the Luebo region (*Batumike et al., 2009*), (b) zircons from the Kafuku and Lubi drill cores (*Delpomdor et al., 2013*) and (c) xenotimes, monazites and zircons from the Kafuku and Lubi drill cores (*this study*). (d) Compilation of all  $^{207}\text{Pb}/^{206}\text{Pb}$  apparent ages (Ga). **Kibara plutonic activity peak, Kibara orogenic cycle, Usagara/Ubende orogeny, Luiza Metasedimentary Complex and Lulua Group.**

**Fig.10.** (a) Geological map of Archean cratons and Proterozoic to Paleozoic belts near the study area. Compilation of  $^{207}\text{Pb}/^{206}\text{Pb}$  apparent ages (Ga) on (b) zircons from the Luebo region (*Batumike et al., 2009*), (c) xenotimes, monazites and zircons in the Lubi drill core (*this study; Delpomdor et al., 2013*) and (d) xenotimes, monazites and zircons in the Kafuku drill core (*this study; Delpomdor et al., 2013*). Modified after *Kadima et al. (2011)* and *Baludikay et al. (2016a)*.

**Fig.11.** Sources of inherited  $^{207}\text{Pb}/^{206}\text{Pb}$  apparent ages (Ga) during the deposition in the Lubi drill core (*this study and Delpomdor et al., 2013*) and in the Kafuku drill core (*this study and Delpomdor et al., 2013*). Diagenetic ages are also shown on the logs. (EMP): Electron MicroProbe; (ICP): ICP-MS. See Fig.10 for legends. Logs modified after *Delpomdor et al. (2013)*.

## 12. Tables

### Table 1

Samples containing monazites, xenotimes or zircons from BI Group used for U-Pb datings

### Table 2

EMP monazite and xenotime analytical data for BI Group. Errors are  $2\sigma$

### Table 3

LA-ICP-MS monazite and xenotime U-Th-Pb isotope data for BI Group

### Table 4

LA-ICP-MS zircon U–Th–Pb isotope data for BI & BII Group

ACCEPTED MANUSCRIPT

<b>Sample</b>	<b>Drill core</b>	<b>RG number</b>	<b>Depth</b>	<b>Formation</b>
KA-80	Kafuku	41370	53.25	BIE2
KA-83	Kafuku	41371	62.2	BIE2
KA-84	Kafuku	41371	78.8	BIE1
KA-95	Kafuku	41378	119.25	BId2
KA-97	Kafuku	41384	172.15	BId1
LU-149	Lubi	57661	113.90	Ble1
LU-69	Lubi	57788	257.00	Blc2
LU-60	Lubi	57791	269.00	Blc2

ACCEPTED MANUSCRIPT

Spot name	F m	Domain	SiO2	P2O5	CaO	Y2O3	La2O3	Pr2O3	Nd2O3	Sm2O3	Ce2O3	ThO2	PbO	UO2	Total	Age (Ma)	2 $\sigma$ error
KA-95-Mnz-01	Bl-d2	rim	1.143	28.086	1.552	0.448	9.422	3.24	2.980	6.26	30.18	<b>3.10</b>	<b>0.15</b>	<b>0.09</b>	<b>86.68</b>	<b>105</b>	13
			1	4	9	1	7	63	7	49	57	<b>45</b>	<b>83</b>	<b>44</b>	<b>80</b>	<b>1</b>	8
KA-97-Mnz-02	Bl-d1	incl in xen	1.459	28.543	0.206	1.831	12.08	2.15	3.055	5.51	29.72	<b>3.44</b>	<b>0.22</b>	<b>0.26</b>	<b>88.50</b>	<b>114</b>	12
			2	1	1	8	75	77	5	95	21	<b>45</b>	<b>01</b>	<b>28</b>	<b>99</b>	<b>9</b>	3
KA-97-Xen-02	Bl-d1	rim	0.566	28.495	0.032	34.25	0.009	0.00		0.55	0.055	<b>0.77</b>	<b>0.08</b>	<b>0.32</b>	<b>65.15</b>	<b>103</b>	21
			3	0	9	22	3	00	NM	07	4	<b>91</b>	<b>71</b>	<b>88</b>	<b>68</b>	<b>9</b>	9
KA-97-Xen-02	Bl-d1	rim-core	0.512	28.364	0.013	34.16	0.000	0.00		0.51	0.054	<b>0.72</b>	<b>0.15</b>	<b>0.68</b>	<b>65.18</b>	<b>111</b>	16
			0	9	1	46	0	00	NM	78	2	<b>63</b>	<b>14</b>	<b>35</b>	<b>78</b>	<b>5</b>	7
KA-97-Xen-02	Bl-d1	core	0.421	29.782	0.014	37.51	0.004	0.01		0.48	0.049	<b>0.46</b>	<b>0.10</b>	<b>0.48</b>	<b>69.34</b>	<b>115</b>	22
			7	7	0	54	2	90	NM	01	0	<b>83</b>	<b>95</b>	<b>45</b>	<b>84</b>	<b>8</b>	9
KA-97-Xen-02	Bl-d1	core	0.918	30.498	0.032	38.08	0.101	0.00		0.78	0.354	<b>0.90</b>	<b>0.20</b>	<b>0.88</b>	<b>72.76</b>	<b>117</b>	12
			3	4	3	17	1	00	NM	42	3	<b>23</b>	<b>54</b>	<b>68</b>	<b>48</b>	<b>2</b>	2
LU-149(1)-Mnz-01	Bl-e1	-	1.157	26.372	1.054	0.189	21.22	0.65	3.547	0.90	29.39	<b>3.20</b>	<b>0.26</b>	<b>0.06</b>	<b>88.03</b>	<b>169</b>	16
			2	2	6	2	77	78	5	97	27	<b>56</b>	<b>27</b>	<b>19</b>	<b>88</b>	<b>7</b>	0
LU-149(1)-Mnz-01	Bl-e1	-	1.286	26.754	1.127	0.173	21.89	0.68	3.736	0.91	29.90	<b>3.15</b>	<b>0.26</b>	<b>0.06</b>	<b>89.96</b>	<b>170</b>	16
			0	6	4	7	08	65	6	76	70	<b>71</b>	<b>15</b>	<b>46</b>	<b>34</b>	<b>8</b>	2
LU-149(1)-Mnz-01	Bl-e1	-	1.405	27.056	1.065	0.171	22.29	0.63	3.891	0.92	29.90	<b>3.12</b>	<b>0.26</b>	<b>0.05</b>	<b>90.79</b>	<b>177</b>	16
			1	0	0	0	25	37	6	22	99	<b>02</b>	<b>76</b>	<b>93</b>	<b>41</b>	<b>5</b>	7
LU-60-Mnz-01-1	Bl-c2	-	0.417	26.719	0.891	2.114	13.09	2.20	4.009	2.23	27.07	<b>3.50</b>	<b>0.29</b>	<b>0.44</b>	<b>83.00</b>	<b>131</b>	10
			9	6	6	6	44	54	8	80	00	<b>08</b>	<b>99</b>	<b>66</b>	<b>86</b>	<b>2</b>	5
LU-60-Mnz-01-2	Bl-c2	-	0.699	29.846	0.814	1.271	13.34	2.13	4.027	2.24	27.68	<b>3.69</b>	<b>0.35</b>	<b>0.73</b>	<b>86.87</b>	<b>126</b>	
			4	9	9	2	93	84	9	40	62	<b>95</b>	<b>89</b>	<b>50</b>	<b>16</b>	<b>8</b>	86
LU-60-Mnz-01-3	Bl-c2	-	1.132	18.175	1.416	2.085	12.78	1.94	4.127	1.99	23.81	<b>3.61</b>	<b>0.38</b>	<b>0.85</b>	<b>72.32</b>	<b>130</b>	
			7	5	1	9	48	60	1	13	39	<b>09</b>	<b>77</b>	<b>47</b>	<b>66</b>	<b>0</b>	80
LU-60-Mnz-03-1	Bl-c2	-	0.328	27.433	1.492	2.067	13.06	1.96	4.329	2.17	25.96	<b>4.69</b>	<b>0.45</b>	<b>0.90</b>	<b>84.86</b>	<b>129</b>	
			5	0	9	4	36	41	4	00	41	<b>41</b>	<b>75</b>	<b>01</b>	<b>47</b>	<b>2</b>	71
LU-60-Mnz-03-2	Bl-c2	-	0.868	27.245	1.596	2.475	12.05	1.81	3.946	2.30	25.99	<b>4.38</b>	<b>0.47</b>	<b>1.08</b>	<b>84.25</b>	<b>127</b>	
			2	6	1	9	89	47	5	22	93	<b>89</b>	<b>34</b>	<b>78</b>	<b>75</b>	<b>9</b>	68
LU-60-Mnz-04-1	Bl-c2	-	0.730	26.435	0.848	0.598	12.78	2.12	2.777	1.43	25.93	<b>4.00</b>	<b>0.23</b>	<b>0.13</b>	<b>78.04</b>	<b>115</b>	11
			2	5	8	6	99	30	7	52	33	<b>04</b>	<b>29</b>	<b>46</b>	<b>01</b>	<b>6</b>	8
LU-60-Mnz-04-	Bl-	-	1.206	27.728	0.773	1.262	12.59	2.10	2.892	1.24	25.22	<b>3.45</b>	<b>0.21</b>	<b>0.10</b>	<b>78.80</b>	<b>124</b>	13



Spot Name	Formation	Domain	Pb (ppm)	Th (ppm)	U (ppm)	Th/U	$^{207}\text{Pb}/^{235}\text{U}$	2 $\sigma$ err	$^{206}\text{Pb}/^{238}\text{U}$	2 $\sigma$ err	$\rho$	$^{208}\text{Pb}/^{232}\text{Th}$ age (Ma)	2 $\sigma$ err	$^{207}\text{Pb}/^{206}\text{Pb}$ age (Ma)	2 $\sigma$ err	$^{206}\text{Pb}/^{238}\text{U}$ age (Ma)	2 $\sigma$ err	Concord. %
KA-80-Xen-02	BI-E2	-	289	70	663	1.1	2.265	0.07	0.164	0.00	0.71	1229	31	1633	74	976	2	60
KA-80-Xen-02	BI-E2	-	376	87	859	1.0	2.923	0.10	0.169	0.00	0.72	1098	29	2037	71	1005	2	49
KA-80-Xen-02	BI-E2	-	118	83	159	0.5	5.381	0.23	0.306	0.00	0.63	2582	93	2066	86	1720	4	83
KA-80-Xen-02	BI-E2	-	402	60	822	0.7	3.487	0.11	0.189	0.00	0.79	1694	42	2151	64	1115	2	52
KA-80-Mnz-05	BI-E2	core	4138	35	2685	13	2.071	0.06	0.175	0.00	0.84	979	22	1338	66	1038	6	78
KA-80-Mnz-03	BI-E2	core	340	40	101	25	2.242	0.12	0.192	0.00	0.51	1312	30	1313	116	1130	3	86
KA-80-Mnz-07	BI-E2	core	404	44	78	64	3.310	0.21	0.198	0.00	0.51	973	23	1978	122	1163	0	59
KA-80-Mnz-11	BI-E2	core	141	72	33	22	6.949	0.41	0.341	0.01	0.57	1797	44	2320	108	1892	5	82
KA-80-Mnz-14	BI-E2	-	1123	73	1189	6.2	2.055	0.06	0.179	0.00	0.85	1061	25	1280	66	1059	5	83
KA-80-Mnz-14	BI-E2	-	9626	62	9179	6.8	2.137	0.06	0.186	0.00	0.84	1127	27	1277	67	1100	6	86
KA-80-Mnz-14	BI-E2	-	8096	47	8527	5.6	2.165	0.06	0.189	0.00	0.84	1160	28	1270	66	1116	6	88
KA-80-Mnz-14	BI-E2	-	8530	51	7854	6.5	2.174	0.06	0.192	0.00	0.83	1158	28	1253	67	1129	7	90



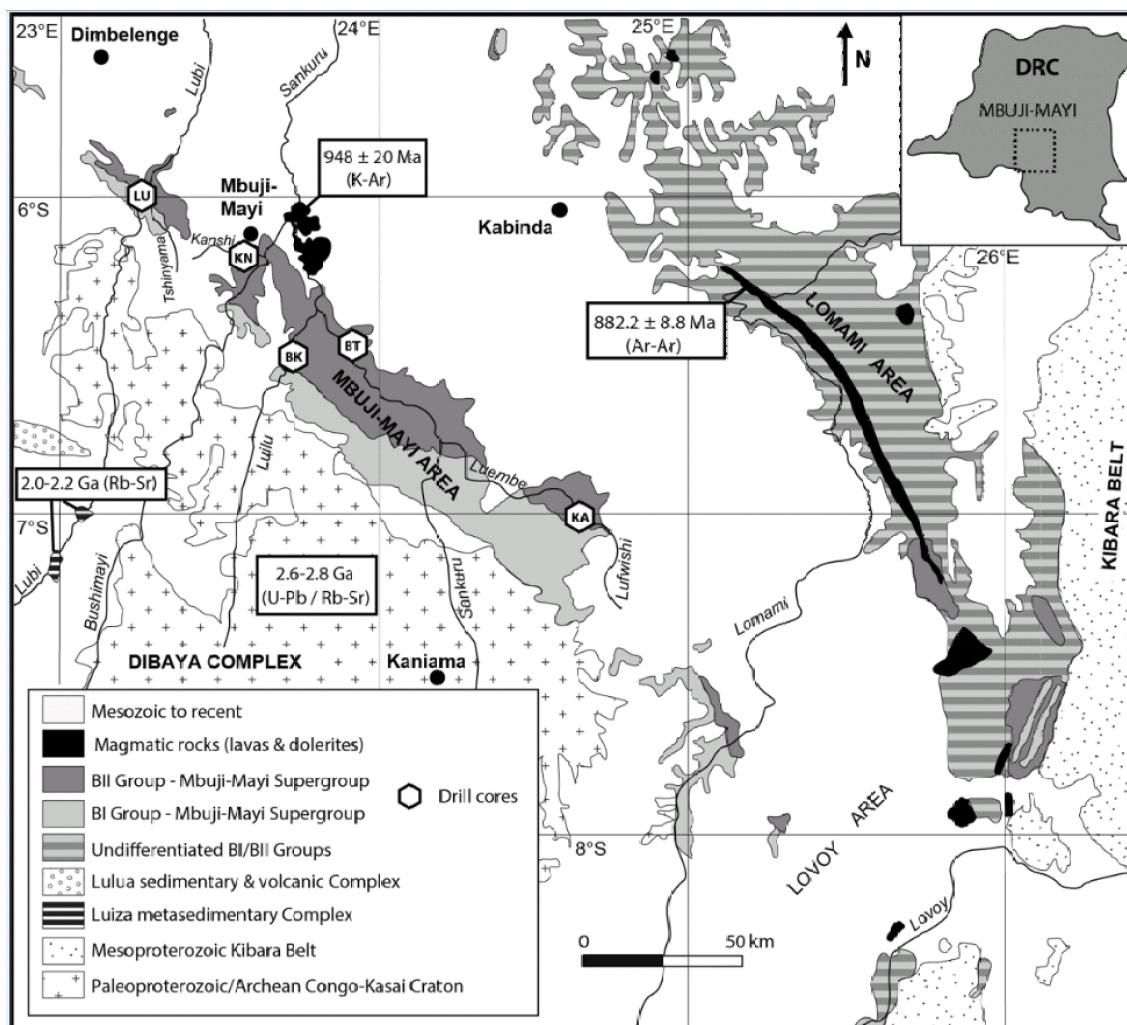
				5														
				16														
<b>KA-84-Mnz-05</b>	BI-E2	core	2745	40	8	2920	5.6	2.673	0.07	0.00	0.91	1053	24	1527	61	1198	2	78
				28														
<b>KA-84-Mnz-06</b>	BI-E2	core	5086	97	7	716	40	5.743	0.15	0.00	0.87	1776	39	1955	60	1922	4	98
				21														
<b>KA-84-Mnz-07</b>	BI-E2	core	2363	07	6	238	89	5.228	0.19	0.00	0.72	1201	27	2074	73	1670	3	81
				15														
<b>KA-84-Mnz-08</b>	BI-E2	core	2652	41	0	1136	14	4.796	0.13	0.00	0.87	1426	31	1952	60	1644	3	84
				28														
<b>KA-84-Mnz-09</b>	BI-E2	rim	3672	09	4	1041	27	2.744	0.07	0.00	0.86	1282	28	1353	65	1333	2	98
				27														
<b>KA-84-Mnz-09</b>	BI-E2	rim	3294	44	6	693	40	2.761	0.07	0.00	0.84	1226	27	1375	66	1326	2	96
				14														
<b>KA-84-Mnz-11</b>	BI-E2	core	2165	66	7	143	102	6.796	0.24	0.01	0.71	1612	35	2150	73	2021	4	94
				28														
<b>KA-84-Mnz-13</b>	BI-E2	rim	6521	63	8	610	47	12.577	0.34	0.01	0.86	2313	49	2746	55	2523	5	92
				43														
<b>KA-84-Mnz-13</b>	BI-E2	rim	1066	63	1	4	878	50	0.39	0.01	0.84	2482	53	2783	57	2658	5	96
				39														
<b>KA-84-Mnz-16</b>	BI-E2	core	5636	18	9	349	112	5.370	0.17	0.00	0.77	1579	34	1998	66	1775	3	89
				53														
<b>KA-95-Xen-01</b>	BI-d2	core	885	16	1411	3.8	1.945	0.05	0.00	0.83	741	17	1189	68	1051	2	88	
				89														
<b>KA-95-Xen-02</b>	BI-d2	core	289	1	676	1.3	1.561	0.06	0.00	0.64	794	22	1029	89	923	2	90	
<b>KA-97-</b>	BI-d1	core	1172	81	390	21	2.758	0.08	0.227	0.00	0.78	1398	32	1384	71	1320	3	95

<b>Mnz-02</b>				29				8		6							0	
<b>KA-97-</b>				31				0.05		0.00							2	
<b>Xen-02</b>	Bl-d1	core	1016	51	1897	1.7	1.967	8	0.177	4	0.83	1029	24	1217	68	1048	4	86
<b>KA-97-</b>				30				0.07		0.00							2	
<b>Xen-01</b>	Bl-d1	core	629	86	1126	2.7	2.190	1	0.179	4	0.77	697	17	1403	72	1060	4	76
<b>KA-97-</b>				36				0.06		0.00							2	
<b>Xen-03</b>	Bl-d1	-	3107	42	5989	0.6	2.346	0	0.204	5	0.94	1276	29	1275	61	1199	6	94
<b>KA-97-</b>				36				0.05		0.00							2	
<b>Xen-03</b>	Bl-d1	-	3779	46	7852	0.5	2.201	6	0.192	5	0.93	1279	29	1274	61	1132	5	89
<b>KA-97-</b>				27				0.05		0.00							2	
<b>Xen-03</b>	Bl-d1	-	3280	76	7408	0.4	2.075	4	0.182	4	0.92	1086	26	1260	62	1079	4	86
<b>KA-97-</b>				34				0.05		0.00							2	
<b>Xen-03</b>	Bl-d1	-	3324	28	7208	0.5	2.121	5	0.185	4	0.93	1153	27	1274	61	1094	4	86
<b>KA-97-</b>				54				0.06		0.00							2	
<b>Xen-Zr-17</b>	Bl-d1	rim	2178	30	3876	1.4	2.451	3	0.202	5	0.93	904	21	1382	60	1187	6	86
<b>KA-97-</b>				24				0.07		0.00							2	
<b>Xen-Zr-17</b>	Bl-d1	rim	740	95	1220	2.1	2.486	2	0.208	5	0.84	807	19	1355	66	1218	7	90
				27														
<b>LU-69-</b>				90				0.06		0.00							2	
<b>Mnz-04</b>	Bl-c2	rim	5202	8	4804	5.8	2.529	8	0.215	5	0.93	1245	29	1320	62	1257	8	95
				30														
<b>LU-69-</b>				95				0.06		0.00							2	
<b>Mnz-04</b>	Bl-c2	rim	5400	3	4932	6.3	2.433	6	0.206	5	0.92	1209	28	1327	62	1210	7	91
				18														
<b>LU-69-</b>				79				0.07		0.00							2	
<b>Mnz-05</b>	Bl-c2	rim	2589	3	1086	17	2.607	6	0.223	6	0.86	1264	30	1315	66	1295	9	99
				22														
<b>LU-69-</b>				64				0.08		0.00							3	
<b>Mnz-05</b>	Bl-c2	core	2884	5	954	24	2.662	1	0.222	6	0.83	1229	29	1363	67	1291	0	95
<b>LU-69-</b>				56				0.09		0.00							3	
<b>Mnz-08</b>	Bl-c2	rim	913	20	444	13	2.815	2	0.223	6	0.78	1420	33	1460	70	1297	0	89
				15														
<b>LU-69-</b>				72				0.08		0.00							2	
<b>Mnz-08</b>	Bl-c2	rim	2238	2	1286	12	2.667	1	0.214	5	0.83	1200	28	1432	67	1251	9	87
<b>LU-69-</b>				42				0.09		0.00							2	
<b>Mnz-02</b>	Bl-c2	core	465	94	267	16	2.205	2	0.179	5	0.64	1013	24	1416	87	1059	6	75

				50														
<b>LU-69-</b>				13				0.07		0.00								2
<b>Mnz-07</b>	Bl-c2	core	4932	1	1611	31	2.532	5	0.200	5	0.85	1012	24	1464	65	1175	7	80
				44														
<b>LU-69-</b>				78				0.32		0.01								4
<b>Mnz-13</b>	Bl-c2	core	9858	1	751	60	11.787	4	0.443	1	0.91	2338	53	2769	53	2362	9	85
				46														
<b>LU-69-</b>				42				0.31		0.01								4
<b>Mnz-13</b>	Bl-c2	rim	9557	2	303	153	11.128	5	0.430	1	0.89	2295	52	2723	55	2305	9	85
<b>LU-69-</b>				52				0.08		0.00								3
<b>Mnz-19</b>	Bl-c2	core	1241	72	1170	4.5	2.887	6	0.234	6	0.84	1482	34	1417	65	1354	1	96
				54														
<b>LU-60-</b>				58				0.07		0.00								2
<b>Mnz-03</b>	Bl-c2	rim	7927	8	5888	9.3	2.632	2	0.202	5	0.90	1169	27	1520	61	1185	7	78
				54														
<b>LU-60-</b>				29				0.06		0.00								2
<b>Mnz-03</b>	Bl-c2	rim	7932	1	5826	9.3	2.522	9	0.204	5	0.90	1171	27	1418	62	1197	7	84

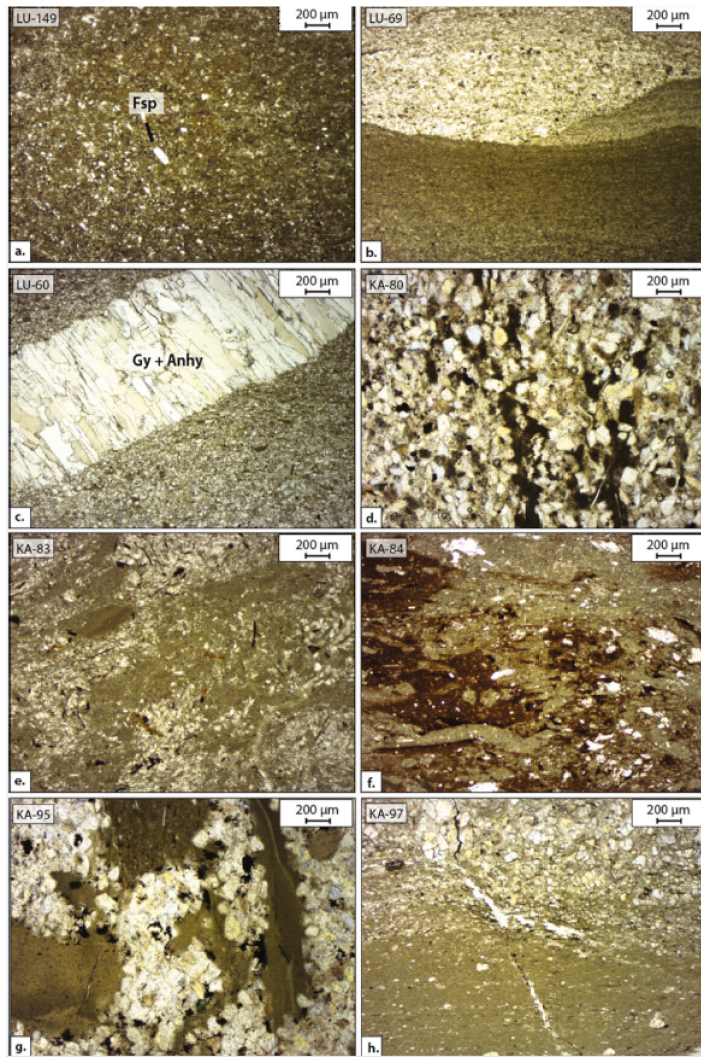
Spot Name	Formation	Domain	Pb (ppm)	Th (ppm)	U (ppm)	Th/U	$^{207}\text{Pb}/^{235}\text{U}$	2 $\sigma$ err	$^{206}\text{Pb}/^{238}\text{U}$	2 $\sigma$ err	$\rho$	$^{207}\text{Pb}/^{206}\text{Pb}$ age (Ma)	2 $\sigma$ err	$^{206}\text{Pb}/^{238}\text{U}$ age (Ma)	2 $\sigma$ err	Conc
LU-149 (1)-Zr-12	Bl-e1	core	210	806	1001	0.8	3.532	0.092	0.199	0.005	0.89	2077	57	1172	25	56
LU-149 (1)-Zr-14	Bl-e1	rim	194	186	416	0.5	11.916	0.298	0.429	0.010	0.92	2838	52	2301	44	81
LU-149 (1)-Zr-14	Bl-e1	rim	67	142	165	0.9	9.880	0.26	0.362	0.008	0.89	2808	54	1993	40	71
LU-149 (1)-Zr-22	Bl-e1	rim	11	30	36	0.8	4.402	0.19	0.252	0.007	0.62	2054	85	1447	35	70
LU-149 (1)-Zr-22	Bl-e1	core	16	47	61	0.8	4.031	0.138	0.221	0.005	0.72	2130	70	1286	29	60
LU-149 (1)-Zr-24	Bl-e1	rim	66	149	503	0.3	1.916	0.05	0.121	0.003	0.88	1876	59	737	16	39
LU-149 (1)-Zr-24	Bl-e1	rim	112	171	767	0.2	2.092	0.053	0.139	0.003	0.89	1786	59	838	18	47
LU-149 (1)-Zr-28	Bl-e1	rim	140	490	1119	0.4	2.062	0.053	0.112	0.003	0.89	2138	57	687	15	32
LU-149 (1)-Zr-38	Bl-e1	core	412	449	1760	0.3	5.017	0.127	0.220	0.005	0.89	2508	55	1284	26	51
LU-149 (1)-Zr-38	Bl-e1	rim	258	280	1341	0.2	3.852	0.098	0.181	0.004	0.88	2397	55	1071	22	45
LU-149 (1)-Zr-36	Bl-e1	rim	23	39	85	0.5	3.312	0.098	0.245	0.006	0.77	1591	68	1410	29	89
LU-149 (1)-Zr-36	Bl-e1	rim	39	83	161	0.5	3.115	0.085	0.229	0.005	0.83	1598	64	1330	27	83
LU-149 (1)-Zr-40	Bl-e1	core	270	304	847	0.4	6.115	0.153	0.306	0.007	0.88	2290	56	1719	33	75
LU-149 (2)-Zr-02	Bl-e1	rim	156	260	296	0.9	12.123	0.314	0.419	0.009	0.87	2906	54	2254	43	78
LU-149 (2)-Zr-02	Bl-e1	rim	159	200	293	0.7	12.940	0.337	0.446	0.010	0.86	2910	54	2376	45	82
LU-149 (2)-Zr-02	Bl-e1	core	98	227	202	1.1	11.068	0.293	0.381	0.009	0.85	2911	55	2081	40	71

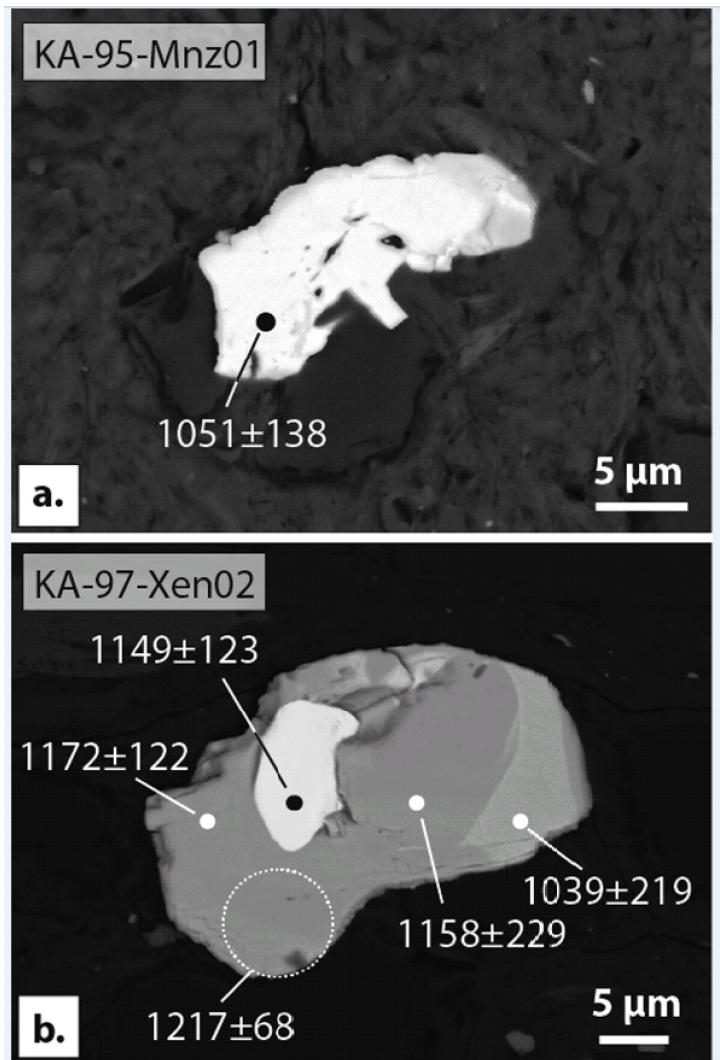
<b>LU-149 (2)-Zr-09</b>	Bl-e1	core	21	57	91	0.6	2.949	0.092	0.215	0.005	0.73	1612	70	1257	26	78
<b>LU-149 (2)-Zr-12</b>	Bl-e1	core	26	80	80	1.0	4.578	0.141	0.273	0.006	0.74	1978	68	1557	31	79
<b>LU-149 (2)-Zr-12</b>	Bl-e1	rim	26	101	87	1.2	3.988	0.13	0.240	0.006	0.71	1967	70	1384	29	70
<b>LU-149 (2)-Zr-06</b>	Bl-e1	core	108	124	485	0.3	3.185	0.084	0.217	0.005	0.82	1737	63	1267	25	73
<b>LU-149 (2)-Zr-04</b>	Bl-e1	core	100	449	319	1.4	4.356	0.119	0.238	0.005	0.79	2138	61	1373	27	64
<b>LU-149 (2)-Zr-04</b>	Bl-e1	rim	90	315	407	0.8	3.599	0.099	0.193	0.004	0.78	2164	62	1139	23	53
<b>KA-83-Zr-01</b>	Bl-E2	core	66	626	701	0.9	1.178	0.045	0.079	0.002	0.68	1769	77	490	12	28
<b>KA-83-Zr-02</b>	Bl-E2	core	49	208	247	0.8	1.927	0.066	0.160	0.004	0.73	1371	74	955	22	70
<b>KA-83-Zr-03</b>	Bl-E2	core	34	101	133	0.8	3.912	0.141	0.222	0.006	0.72	2070	72	1291	30	62
<b>KA-83-Zr-04</b>	Bl-E2	rim	93	674	992	0.7	1.271	0.039	0.084	0.002	0.80	1794	66	520	12	29
<b>KA-83-Zr-04</b>	Bl-E2	rim	113	385	807	0.5	1.942	0.06	0.129	0.003	0.80	1793	65	779	18	43
<b>KA-83-Zr-06</b>	Bl-E2	core	39	93	220	0.4	3.040	0.108	0.167	0.004	0.71	2123	71	997	23	47
<b>LU-60-Zr-05</b>	Bl-c2	rim	52	567	253	2.2	2.017	0.058	0.148	0.003	0.81	1605	65	889	19	55
<b>LU-60-Zr-14-2</b>	Bl-c2	core	13	28	38	0.7	5.153	0.173	0.281	0.007	0.72	2140	69	1595	34	75
<b>LU-60-Zr-14-2</b>	Bl-c2	rim	23	49	71	0.7	4.193	0.128	0.282	0.007	0.76	1764	67	1600	33	91
<b>LU-60-Zr-14-1</b>	Bl-c2	rim	50	330	376	0.9	1.678	0.047	0.126	0.003	0.79	1561	66	764	16	49
<b>LU-69-Zr-11</b>	Bl-c2	core	19	190	185	1.0	1.094	0.042	0.089	0.002	0.62	1406	84	550	13	39
<b>LU-69-Zr-09</b>	Bl-c2	core	125	553	780	0.7	2.064	0.055	0.142	0.003	0.83	1729	62	853	18	49
<b>LU-69-Zr-21</b>	Bl-c2	rim	33	149	173	0.9	2.202	0.074	0.176	0.004	0.69	1437	76	1047	22	73
<b>LU-69-Zr-07</b>	Bl-c2	core	40	98	206	0.5	2.318	0.064	0.184	0.004	0.80	1456	66	1088	22	75
<b>LU-69-Zr-15</b>	Bl-c2	rim	33	49	160	0.3	2.401	0.073	0.208	0.005	0.74	1284	73	1219	25	95
<b>LU-69-Zr-15</b>	Bl-c2	core	32	54	141	0.4	2.581	0.075	0.222	0.005	0.77	1303	70	1290	26	99
<b>LU-69-Zr-01</b>	Bl-c2	core	17	202	182	1.1	1.160	0.054	0.084	0.002	0.54	1636	96	518	13	32
<b>LU-69-Zr-03</b>	Bl-c2	core	13	102	61	1.7	2.405	0.14	0.152	0.004	0.50	1881	114	910	24	48

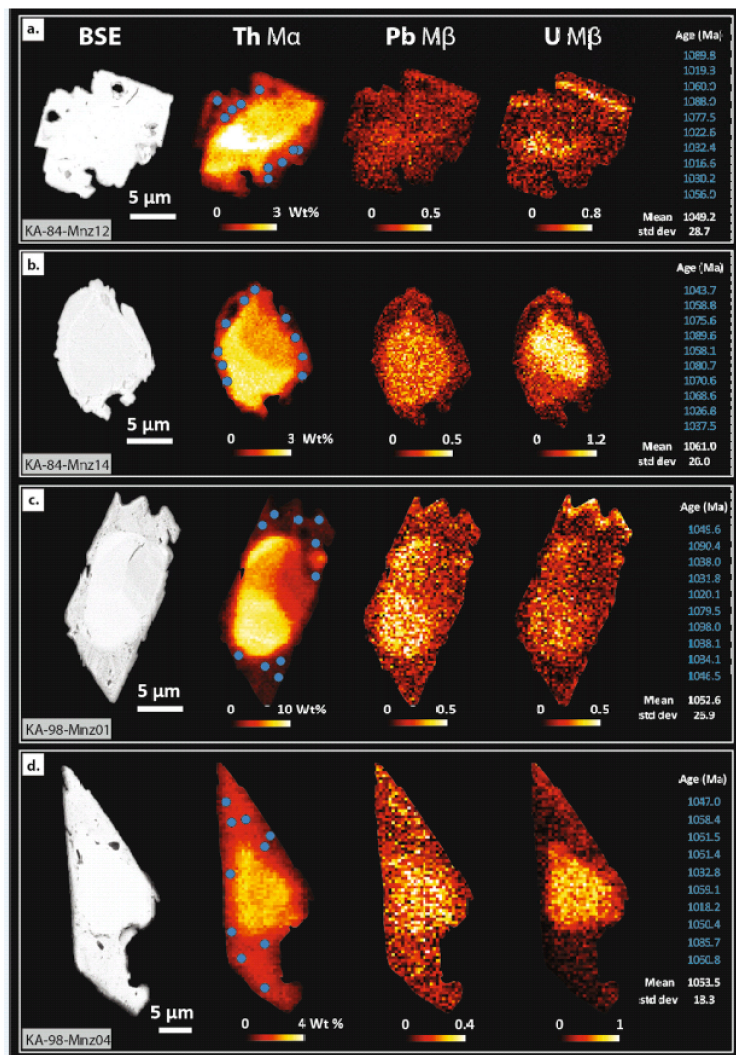




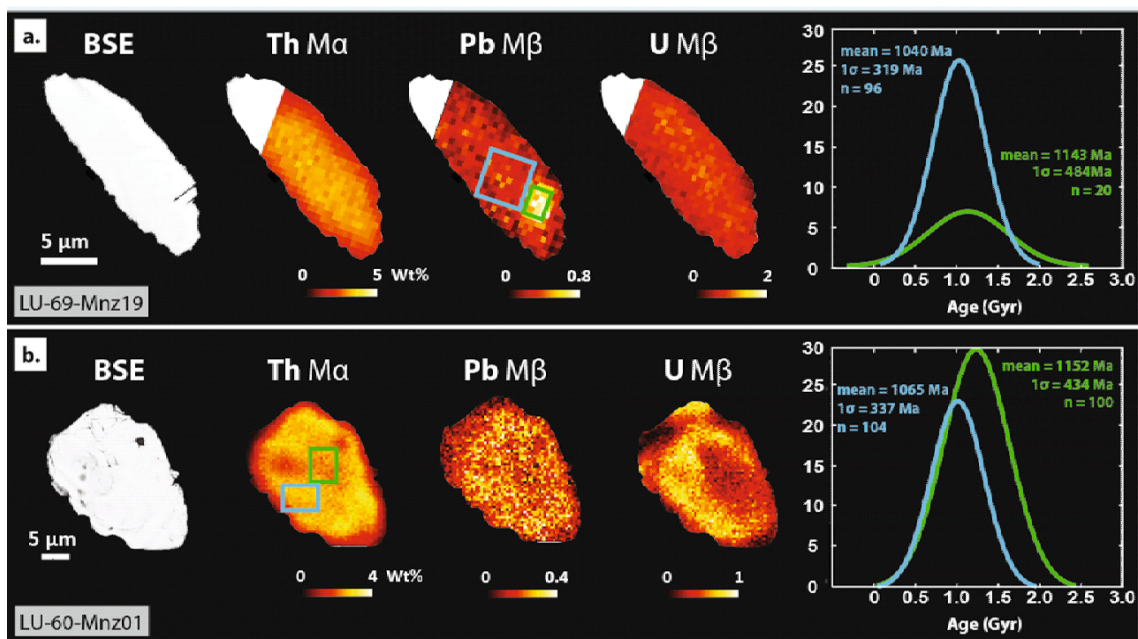


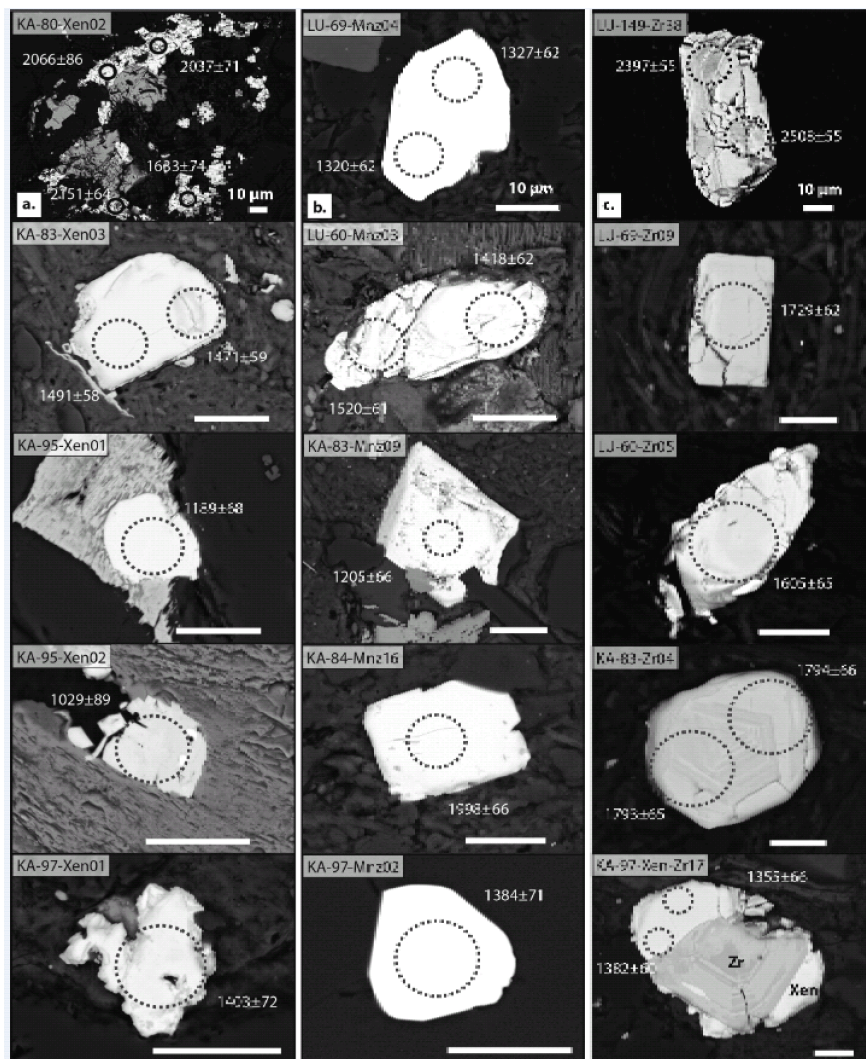


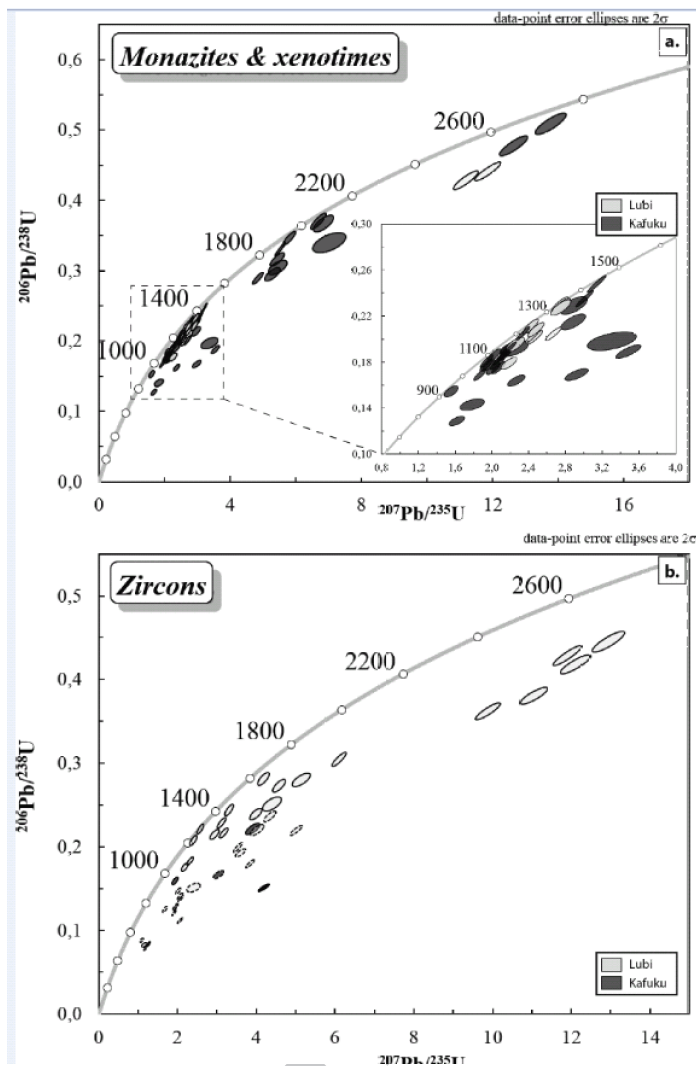


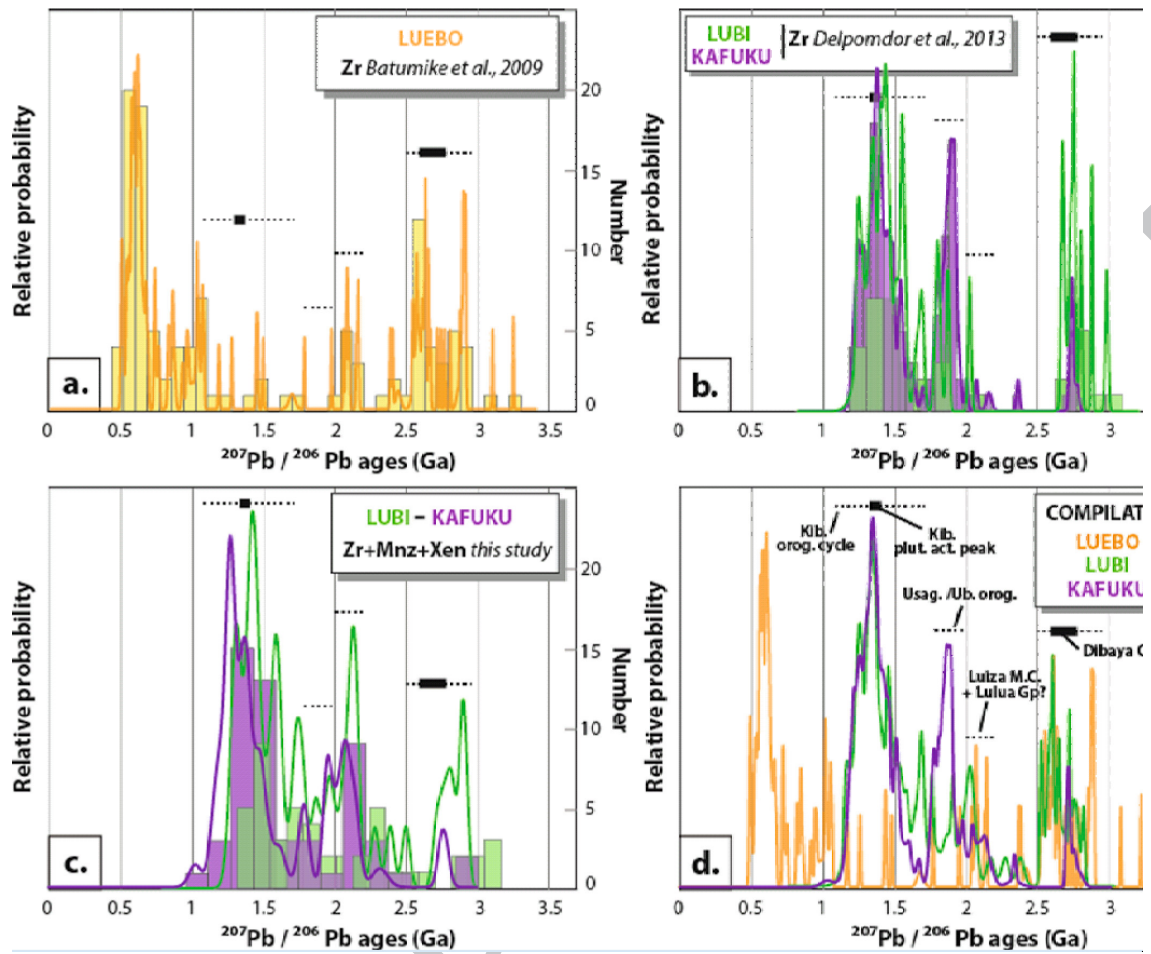






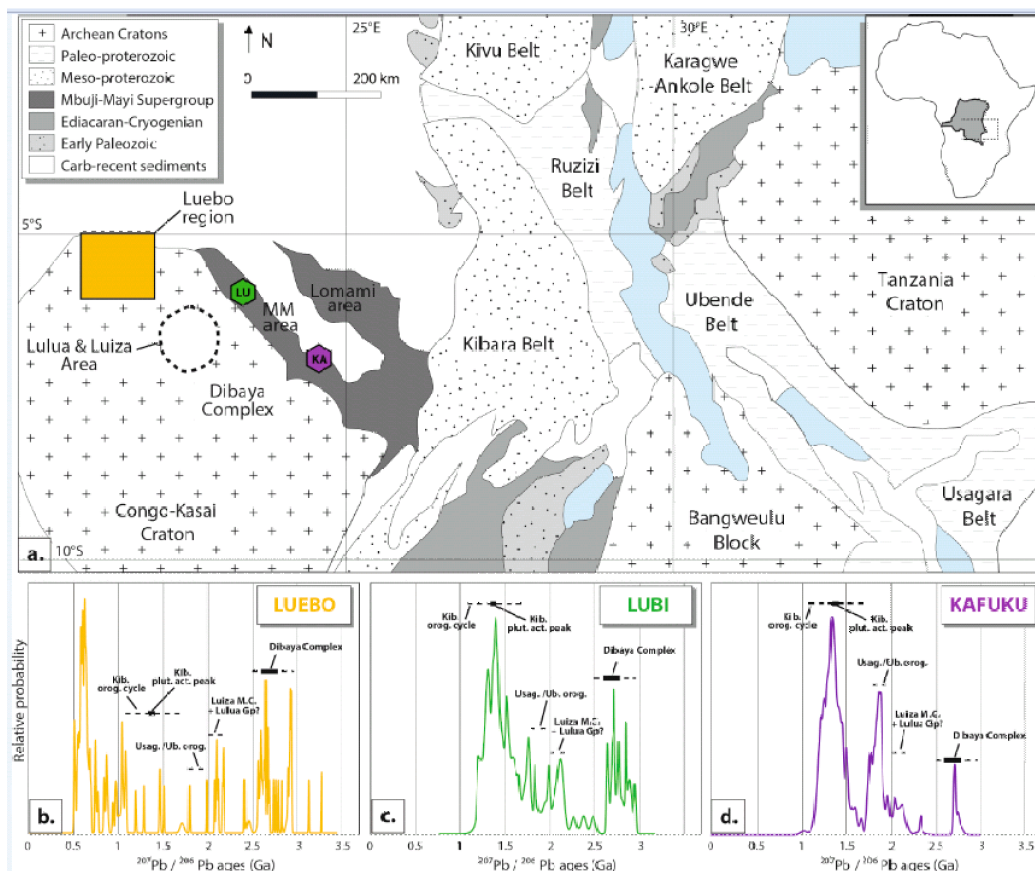


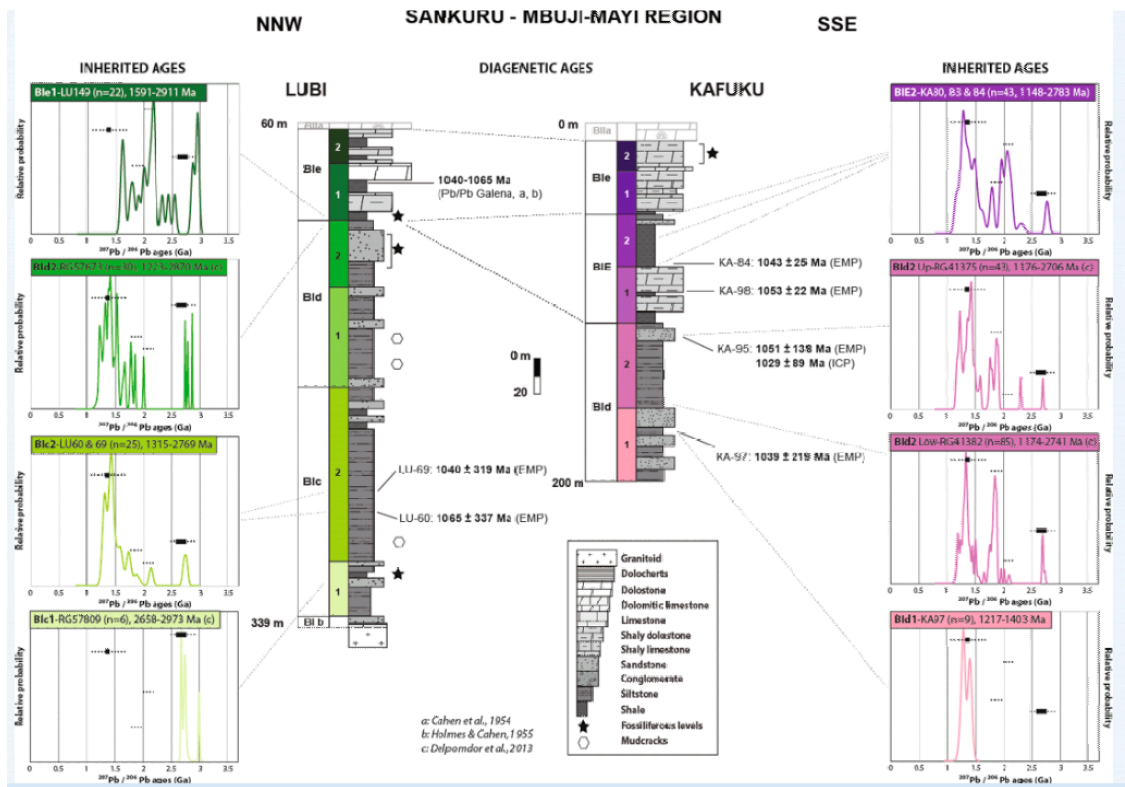




ACCEPTED TEL







ACCEPTED MANUSCRIPT